



Partial discharge measurement on cable termination without coupling capacitor

Szilárd Lipták

2013

Advisers: Zoltán Ádám TAMUS, Ph.D.
Associate Professor
Budapest University of Technology and Economics

Reinhold Bräunlich, Ph.D.
General Manager
FKH Fachkommission für Hochspannungsfragen

Table of content:

Summary	1
1. Introduction, Problem formulation	2
2. Summary of previous works [6]	4
3. PD Measurement circuits	7
3.1 Laboratory measurements of the electric model	7
3.1.1 Model setup	7
3.1.2 Specification of the measurement equipment.....	8
3.1.3 Measurement results.....	8
3.2 On-site measurements.....	10
3.2.1 Specification of the measurement equipment and the object under test	10
3.2.2 Measurement results.....	10
4. Simulation in Micro-Cap	15
4.1 PD Calibrators	15
4.1.1 Power Diagnostix CAL1A calibrator	16
4.1.2 Power Diagnostix CAL1E calibrator	18
4.2 TT-SI 9001 Differential probe.....	20
4.3 Model for the laboratory measurement	22
4.3.1 Definition of inductances.....	22
4.3.2 Definition of resistances.....	22
4.3.3 Definition of stray capacitances	23
4.3.4 Parameter fine-tuning	24
4.3.5 Comparison of measurement and simulation results	27
4.4 Model for the on-site measurements.....	30
4.4.1 Definition of inductances.....	30
4.4.2 Definition of resistances.....	30
4.4.3 Definition of stray capacitances	31
4.4.4 Definition of the stress cone model.....	31
4.4.5 Definition of cable shielding model.....	31
4.4.6 Parameter fine-tuning	32
4.4.7 Comparison with HV test installation.....	34
5. Analysis of created models	36
5.1 Analysis of frequency response	36
5.2 Analysis of stray capacitance variations.....	38
5.2.1 $C_{\text{ground-shielding}}$	38

5.2.2	$C_{\text{Shielding-Core}}$	39
5.2.3	$C_{\text{Core-Ground}}$	40
5.3	Analysis of variations in the terminal's length.....	41
5.4	Analysis of the measurement cables' length.....	42
5.5	Analysis of the termination with capacitive divider.....	43
5.5.1	Influence of the divider's capacitance.....	43
5.5.2	Influence of the HV connection's length.....	43
6.	Conclusion.....	44
7.	References.....	45
	Appendices.....	46
I.	Appendix: Results of the laboratory model measurements.....	46
II.	Appendix: Results of the on-site measurement with HV test installation.....	47
III.	Appendix: CAL1A measurement results and comparison of simulation with different loads.....	48
IV.	Appendix: CAL1E measurement results and comparison of simulation with different loads.....	49
V.	Appendix: Datasheet of the TT-SI 9001 Differential probe.....	50
VI.	Appendix: Parameter fine-tuning to the Laboratory model.....	51
VII.	Appendix: Blueprint of HE3870-0 cable termination.....	52
VIII.	Appendix: Datasheet of the XDRCU-ALT 500/290 kV XLPE Cable.....	53

Summary

In the case of modern XLPE insulated High-voltage cables, the most common source of failure is the incorrect assembly of joints and cable terminations. In such cases, due to the local high concentration of the electric field, so called partial discharges (PD) can occur. The solid polymer insulations are particularly sensitive to partial discharges and the failure may rapidly lead to breakdown of the insulation. The breakdown of such vital parts of the transmission system may lead to considerable financial losses. Therefore the partial discharge measurement nowadays plays an even greater role of high voltage diagnostics.

The practice shows that the coupling capacitor, which is necessary for the partial discharge measurement, is not always possible to install, especially when the cable termination is on a high scaffold or is hard to approach. Lacking coupling capacitor, the PD decoupling circuit is closed only through the stray capacitances of the termination, thus the requisites of the IEC 60270 are not fulfilled. Based on theoretical considerations, satisfactory signal to noise ratio only on higher frequencies can be achieved. Despite this, during on-site measurements it was possible to reach satisfactory sensitivity with the background noise staying below 20 pC. Nevertheless the measurement error of the apparent charge is uncertain.

The aim of the current research is to make statements that can be utilised by the host-company during on-site measurements. In the first stage of my work I built a digital model based on an electric termination model using Micro-Cap 9 software tool¹. Within the frames of an on-site measurement, it was possible to take measurements of an actual cable termination. Based on these measurement results and the experiences gained during the construction of the laboratory model, a digital model of the termination was created. Following the validation of the created models, a series of simulations were done, investigating the main factors of measurement sensitivity. I investigated the effect of the shape and dimensions of the termination and the measurement setup. I also looked into possible ways of increasing the sensitivity. The research showed that without coupling capacitor sufficient sensitivity may be reached with filter midfrequencies above approximately 2 MHz. The measurement error may account as much as 50%. This is due to the fact that in the most frequently used frequency range of 5-10 MHz a real partial discharge has a much lower amplification than the calibration charge.

1 MicroCap ver. 9: Spectrum Software, 1021 South Wolfe Road, Suite 130, Sunnyvale, CA 94086-8874

1. Introduction, Problem formulation

The reliability of the high voltage equipment is a key question in modern electricity supply and the reliability of the transmission and distribution systems is always defined by the reliability of the weakest link. This weakest link is usually the termination of high voltage cables. In comparison with the cables themselves, the terminations are consisted of many more parts and assembled on-site, therefore the controlling possibilities are limited and the probability of malfunction is higher. [1] Typical assembly failures include wrong position of the stress cone, left void or left pollutant [2]. At the site of such assembly mistakes so called partial discharges (PD's) occur, eventually resulting in the complete breakdown of the equipment. To prevent the outage of such vital parts of the energy system, partial discharge measurements are made after the installation of a new equipment or after a major modification.

The definition according to the IEC 60270 is „localised electrical discharge that only partially bridges the insulation between conductors and which can or can not occur adjacent to a conductor” [3]. There are many sorts of partial discharges: corona discharges, surface discharges, void discharge, treeing, etc. From a measuring point of view two categories can be defined: external discharges and internal discharges. The external discharges (typically corona) are appearing just on the surface of inductors in the open air and thus not damaging the insulation material in contrast with the internal discharges. PD diagnostics usually relies on the detection of the different energy conversion processes (optical, acoustical, electromagnetic or chemical) that occur during a partial discharge. In this work I focus only on the electrical measuring methods.

Figure 1-1 shows the typical circuit representation of a partial discharge. Functions like a voltage-dependent switch, discharging the C_1 capacitance's charge. In ideal case it appears as an exponentially decaying i_1 current signal, where the voltage peak is proportional to the discharge. Partial discharges are conventionally characterised by the so-called apparent charge, which is defined by the IEC 60270 [3] so “if injected within a very short time between the terminals of the test object in a specified test circuit, would give the same reading on the measuring instrument as the PD current pulse itself.” The apparent charge is not equal with the actual charge locally involved in the discharge process, because that cannot be measured from the two terminals. The apparent charge is simply C_2/C_1 times greater than the real charge. Since the ratio is only a constant, it can be well used to characterise the intensity of the partial discharge for a defined case.

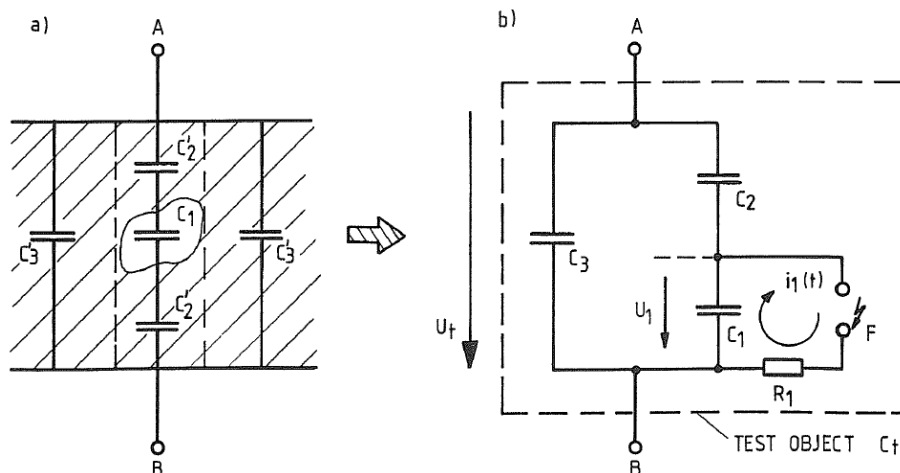


Figure 1-1: (left) insulation void cross-section (right) equivalent circuit diagram [4]

Equation 1-1 shows that the apparent charge can be expressed with the voltage drop across the two terminals. It means the apparent voltage is also a good carrier of information, since the difference is also just a constant. This work is also going to use the measurable voltage to describe the partial discharge and not the conventional apparent charge.

$$q = \left(C_3 + \frac{C_1 * C_2}{C_1 + C_2} \right) * \Delta U_T$$

Equation 1-1: Relation between the apparent charge and measurable voltage [5]

A PD measuring circuit is normally consisting of a coupling capacitor, a coupling quadrupole, a coaxial cable and a measuring instrument. The role of the coupling capacitor is to supply the measurable current, which is compensating the partial discharges in the object under test. Ideally $C_{\text{coupling}} \gg C_{\text{test}}$, but such a great capacitance would mean a too great demand for the power source and could not be economically justified. Normally, the waveform of the discharge pulses is conditioned in various wide-band or narrow-band filters to gain noise immunity, but in this work the signal is not going to be altered. As [4] remarks “Although direct detection of short duration PD current pulses is usually not performed in practical applications, such measurement can frequently supply important information concerning the discharge process in a test object.” Thus during this work we may have a low noise-immunity, but gain more information about the test setup. During the field application, the findings of this work can be used and higher signal to noise ratio can be achieved.

To define the relation between the measured voltage and the apparent charge, the test circuit must be calibrated. It is usually done with a calibrator that can inject a known amount of charge to the object under test. Chapter 4.1 deals with calibrators in detail. A modern PD measuring circuit can display the apparent charges of partial discharges as a function of their phase. The various insulation defects have different image and thus the source of PD's can be very well identified.

Based on the practical experience of the FKH, it is often not possible to install the coupling capacitor because the cable termination is on a high scaffold or is hard to approach. Lacking coupling capacitor, the PD measurement circuit is closed only through the stray capacitances of the termination, thus the requisites of the IEC 60270 are strictly speaking not fulfilled. Since the measuring circuit is closed by only stray capacitances, we would expect a very low sensitivity. Despite this, during on-site measurements it was possible to reach satisfactory sensitivity with the background noise staying under 20 pC. Nevertheless it is uncertain with what error the apparent charge is measured in practice.

Therefore the aim of this work is the transient analysis of a PD measuring circuit without coupling capacitor, investigate the main influencers of measurement sensitivity and draw practical conclusions that may be implemented during other field measurements. For this analysis, a new digital model of termination has been developed and the results of the simulation have been validated by the laboratory model of a termination.

2. Summary of previous works [6]

The current work is a direct continuation of another intern's previous work. In this chapter I detail the progress of this preliminary work, focusing on the parts, which are relevant for this report. I also would like express my gratitude to the previous intern, Ossi Bergius for his efforts, which laid the foundations of my work.

He constructed a laboratory model of a cable termination, which can be seen on Figure 2-1 a). The basic concept of the electric model is excellent, although some side effects were not taken into account properly. The optimisation and current setup of the electric model is going to be detailed in the following chapter. The foregoing work contains measurements to determine the stray capacitances between the different parts of the model, as it can be seen on Figure 2-1 b). Since the stray capacitances play a very important role in the model, the used measuring technique proved to be insufficient. Chapter 4.3 deals with this problem in detail, presenting a more precise measuring method.

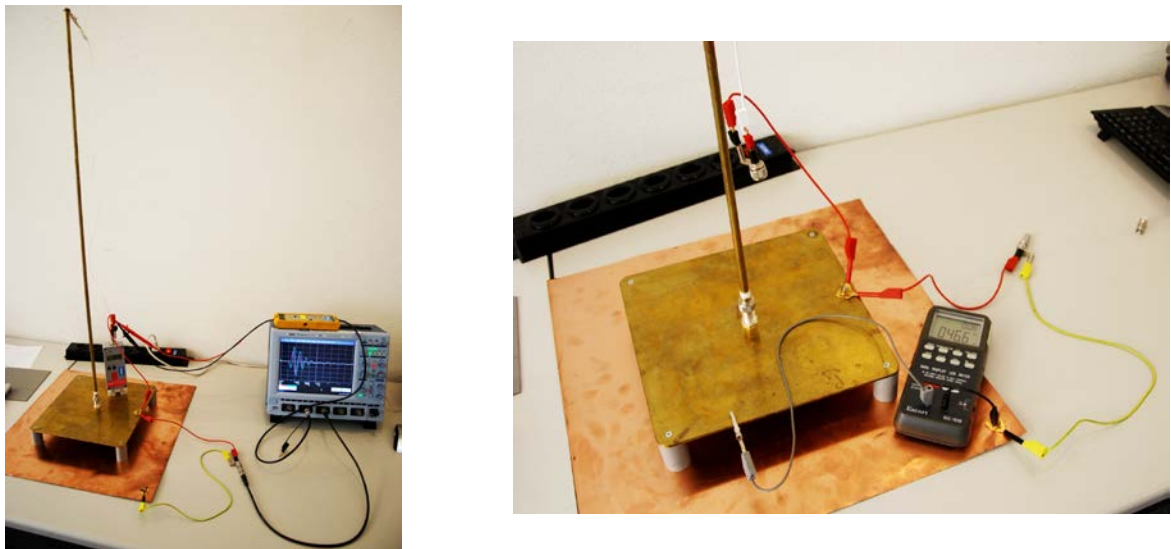


Figure 2-1: (left) Original PD measurement setup (right) Original stray capacitance measurement setup

In the previous work a digital model was created using Micro-Cap 9 software tool, Figure 2-2 presents the resulting circuit. The main components of the circuit are the same as in the present case. An ideal PD source for simulations was used, which however did not correspond to the used calibrator used. The report contains the remark: “the structure of the calibration equipment is not well known and thus it is impossible to build an accurate model for the calibrator.”[6] Therefore the characteristic of the PD calibrator is going to be thoroughly investigated in chapter 4.1.

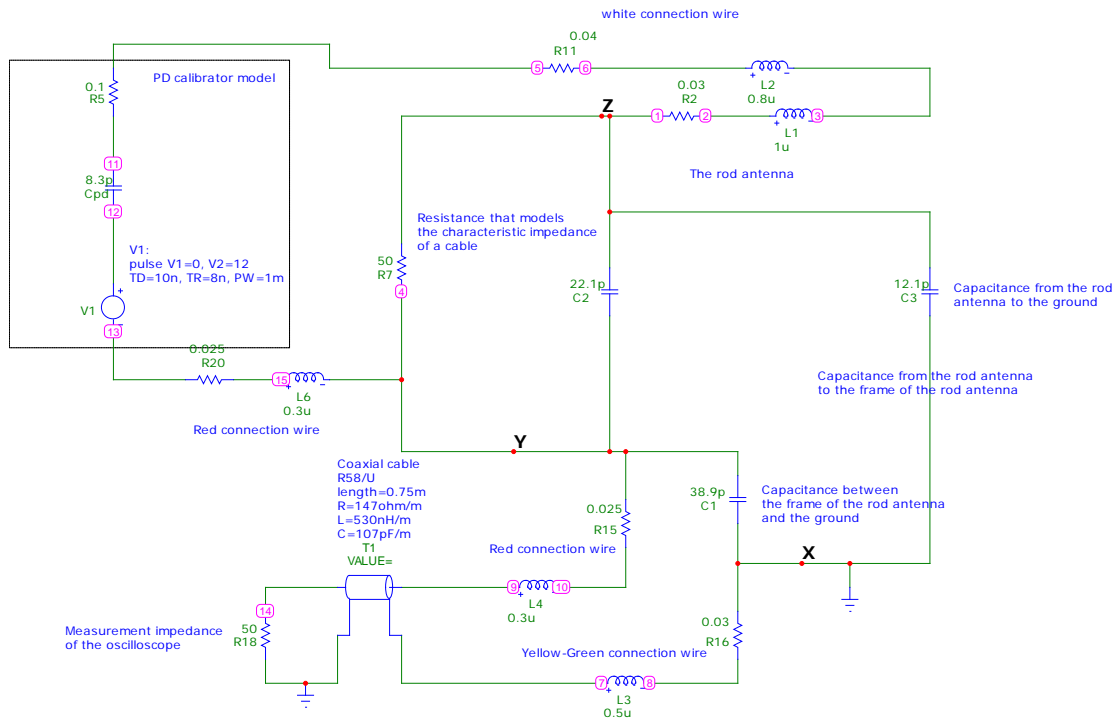


Figure 2-2: Digital model of the laboratory setup

On Figure 2-3 the comparison between the measurement results and the simulation are displayed. The course of the simulation is similar to the measurement, but the attenuation and the angular frequency differ. The later refers to an insufficient matching of the product of inductance and capacitance, which might be due to the measurement uncertainties. He commented the difficulties of defining the model parameters: "It is almost impossible to get the simulation results to match the laboratory measurements. Just a small difference in circuit values changes the output."[6]

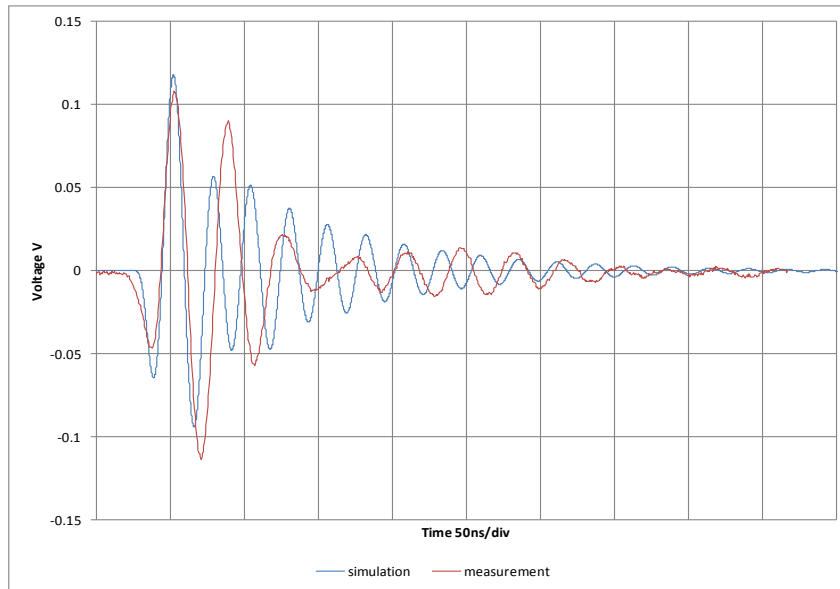


Figure 2-3: Comparison of Laboratory measurement and model

The previous intern also participated on an on-site measurement session and started to develop a circuit model Micro-Cap, but never finished it. An other part of his work, which was also used for comparison during my work, is the field calculation in Electro 4.1. An x-rotational model of the cable termination was used to calculate the capacitances between the different parts of the model (cable core, shielding and the ground). Figure

2-4 shows the used field calculation model. During the field calculations were also investigated other setups, aiming to find ways to increase or to decrease certain stray capacitance. The effect of these modifications to the measurement sensitivity is going to be simulated in chapter 5.2.

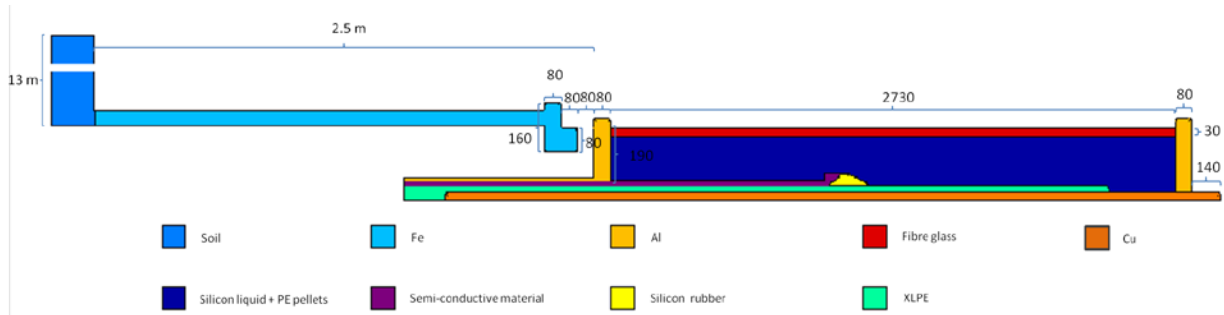


Figure 2-4: Field calculation model of the cable termination

This previous work proved to be a valuable foundation for my activity, but in this unfinished state unable to make conclusions on its own.

3. PD Measurement circuits

The following chapter aims to present the two PD measurement circuits, which were used to create the Micro-Cap models. The first part of this chapter concentrates on the laboratory model and the second part details the on-site measurement.

3.1 Laboratory measurements of the electric model

The laboratory model was constructed to have similar characteristics as an actual cable termination. The aim of the measurement was to gain insights into the typical parameters of the terminations and to utilise this knowledge at the real on-site measurement. In contrast to an actual high voltage cable termination, the parameters could be all measured and changed in the laboratory model.

3.1.1 Model setup

As I introduced in the previous chapter, the original model was constructed within the frames of an other internship. There were a number of disadvantages with the original model (unreliable contact resistances, mechanical weakness) that were improved in this work.

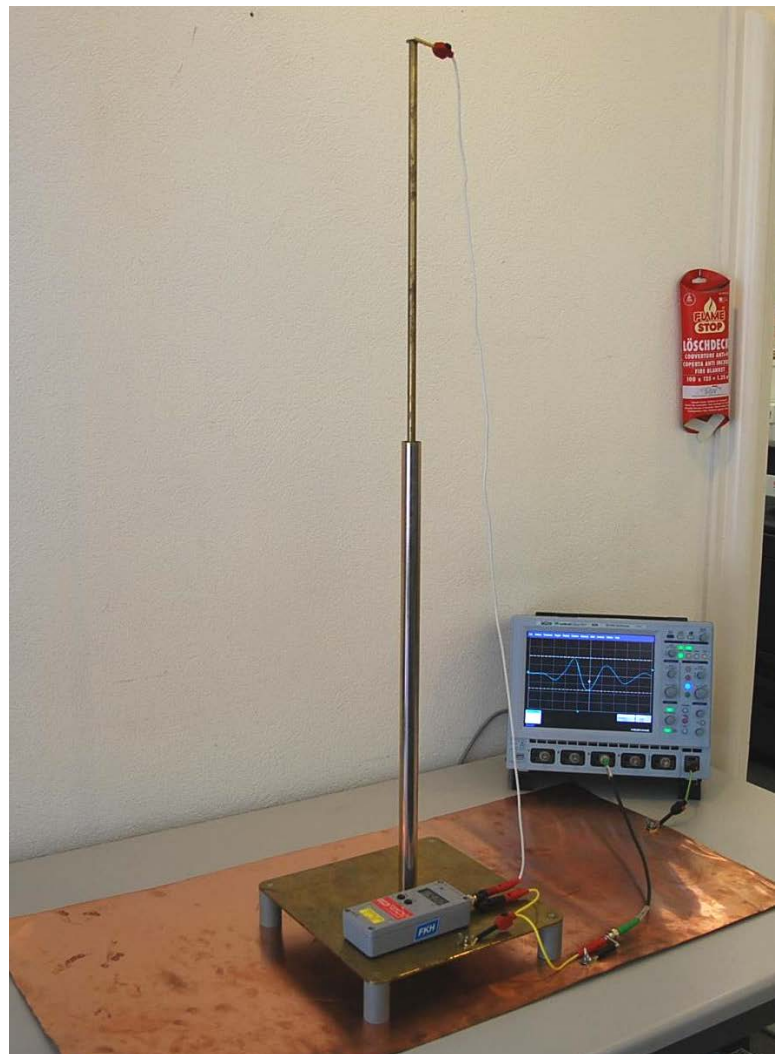
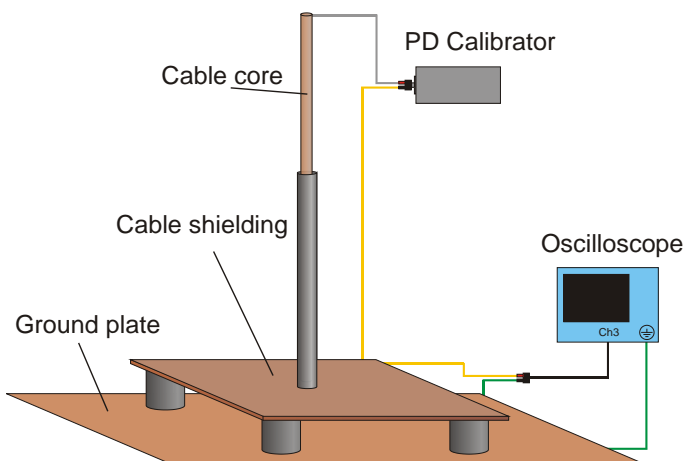


Figure 3-1: The electric laboratory model of a cable termination

Figure 3-1 shows the final state of the model. It is consisted of three main parts: the cable core, the cable shielding and the ground plate. A metal pipe is simulating the stress cone in the termination, and is connected to the cable shielding plate. The cable shielding and the ground plate are separated using four plastic legs. The cable core and the shielding plate were constructed in a way that there is a BNC plug between them. This way it is possible to short it, to open it or to place any other resistance between them. During all the measurements a 50Ω resistance was connected between the core and the shielding, representing the 50Ω characteristic impedance of a long cable. The ground plate is well-grounded through a short cable to the ground of the oscilloscope. The calibrator was placed on the shielding plate and connected to the corresponding part by the shortest cables possible.

There were a number of developments on the model compared to its original state. The metal pipe was replaced with a longer and thinner version in order to increase the stray capacitances. The rod-plate connection was replaced with a mechanically stronger peace and it was also rasped to provide better contact between the plate and the rod. (Previously the contact resistance was relatively high and unreliable.) A proper connection was soldered to the end of the cable core and all cables were custom-made to reduce the stray inductances. The ground plate was also replaced with a bigger one to further increase the stray capacitances. The measurement was so sensitive that even such factors had an influence, like which cables touch each other, the position of the PD calibrator or the RLC meter. To make measurement results comparable, the position of all devices was marked and they were always placed in the exact same position.

3.1.2 Specification of the measurement equipment

- Lecroy Wavesurfer 424 200 MHz oscilloscope

The input impedance was set to be 50Ω to couple the characteristic impedance of the cable. A 1.5 bit noise filter was set that have the -3 dB cut-off frequency at 121 MHz.

- RG 58A/U 40 cm coaxial cable with 50Ω characteristic impedance
- Power Diagnostix CAL1A PD calibrator – it is going to be detailed in chapter 4.1.

3.1.3 Measurement results

During the measurement the background noise was mainly 2 mV with a frequency over 40 MHz. To represent the noise, but also to let the main signal be seen, always 4 measurement data were overlapped on each other. The measurement was performed using different calibration charges (10 pC, 20 pC, 50 pC and 100 pC) and a similar trend could have been observed, like on Figure 3-2.

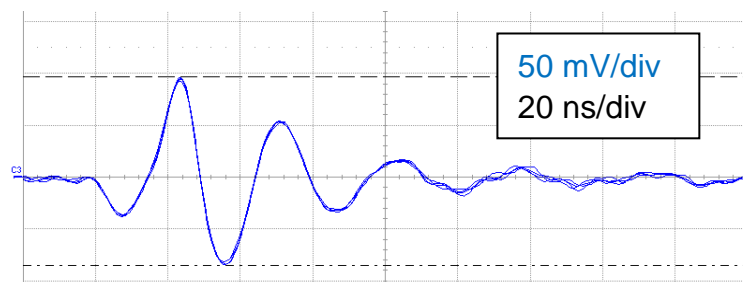


Figure 3-2: Measurement result of the electric model using 50 pC

Appendix I shows all the other measurement results. Figure 3-3 is a summary of those measurements, showing the largest positive peak and the largest negative peak as a function of the injected charge. As it was described in the introduction, it can be clearly

seen that the voltage peak value is almost linearly proportional to the charge. Unfortunately there are also nonlinear attributes of the function, like the behaviour of the first negative swing. (These effects are going to disappear at the on-site measurements.) It proves that a linear model is suitable to produce the same sort of behaviour. To best match all measured data, the 50 pC measurement is going to be used for the simulation.

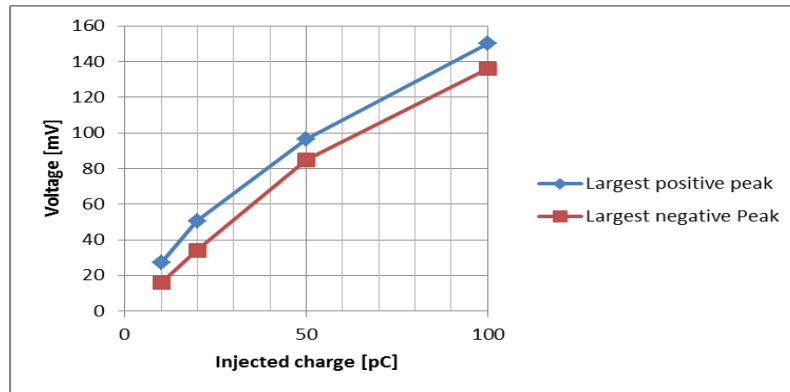


Figure 3-3: Linearity of the measurement results with the electric model

3.2 On-site measurements

The on-site measurement took place at the Water Power Plant Nendaz (Valais, Switzerland), after a voltage test and partial discharge inspection, performed by FKH. Since the time frame for these measurements were very tight, only a limited number of measurements were possible during the disassembly of the installation. As it can be seen on Figure 3-4, a high voltage cable was above the measurement site, inducing great noise in addition to the noise of the substation. This made it necessary to use a different PD calibrator on-site, than in the laboratory. During the measurements special 80 H, high inductance coils were used, which poses a serious challenge in simulation as we will see in chapter 4.4.7.

3.2.1 Specification of the measurement equipment and the object under test

The HV test setup can be seen on Figure 3-4.

- Lecroy Wavesurfer 424 200 MHz oscilloscope with the same settings as in the previous chapter
- RG 58A/U 4 m coaxial cable with 50 Ω characteristic impedance
- Power Diagnostix CAL1E PD calibrator – detailed in chapter 4.1.
- TT-SI 9001 differential probe – detailed in chapter 4.2
- “Obelix” Step-up transformer
- “Trup 3” frequency converter
- 2*80 H HV coils in series (resulting 170 H inductance)
- Capacitive divider primary side: 4*3 nF in series (resulting 0.75 nF)
- Capacitive divider secondary side: 1500 nF

Object under test:

- 430 m XDALW-T 1*400mm² 275/160 kV XLPE cable – The datasheet of a cable with similar construction can be seen in appendix VIII. The calculations were based on this datasheet. The datasheet was provided by the constructor, Brugg Kabel.
- HE3870-0 1*400mm² 275/160 kV cable termination - The blueprint of the termination is to see in appendix VII.

3.2.2 Measurement results

The measurements were performed during two stages of the disassembly process: with the HV test installation and without them. The main harmonic of the background noise is 8 mV at 90 MHz. The Calibrator was set to 0.5 nC, 1 nC, 5 nC and 50 nC. The different measurement data were superimposed on each other in this case as well.

3.2.2.1 Measurement with HV test installation

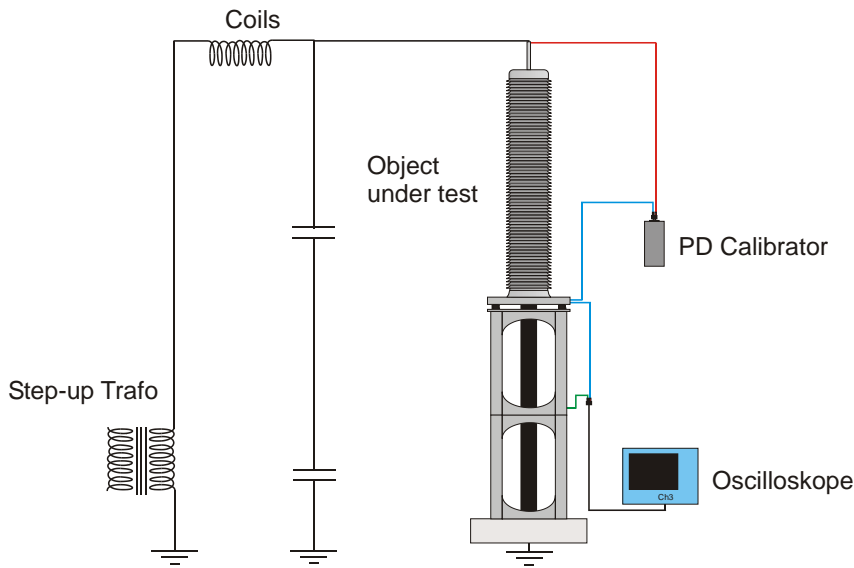


Figure 3-4: The on-site measurement setup with the HV test installation

Figure 3-5 shows the trend of the function at 5 nC. Appendix II shows the other measurement results as well.

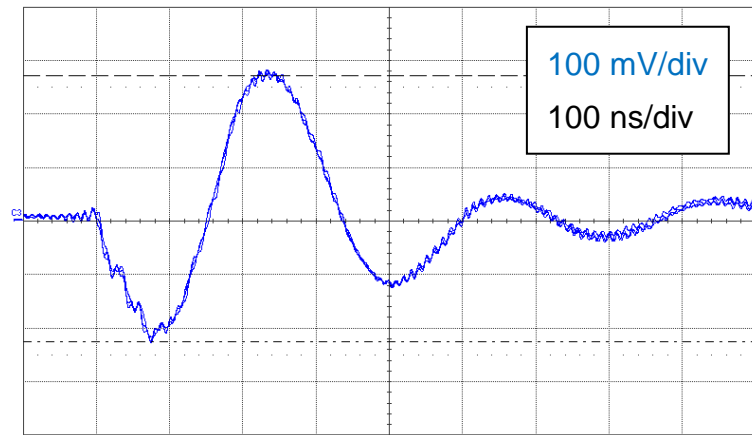


Figure 3-5: Measurement results of the on-site measurement with HV installation at 5 nC

Figure 3-6 shows the linearity of the measurement. It shows the linear dependency of the voltage peak even better, than the laboratory measurements. Here the 5 nC case was selected to be the basis of simulation.

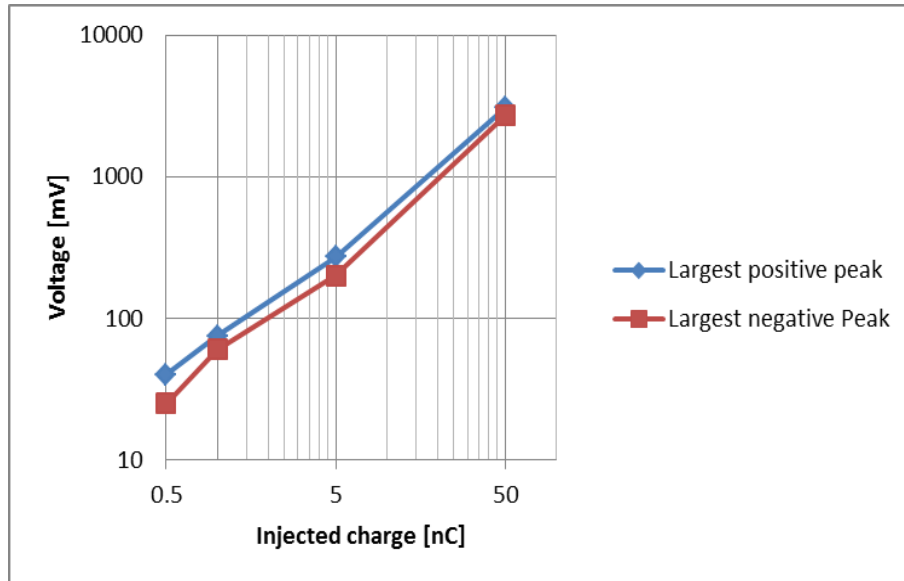


Figure 3-6: Linearity of the measurement results with the HV installation

3.2.2.2 Measurement of the separate cable termination

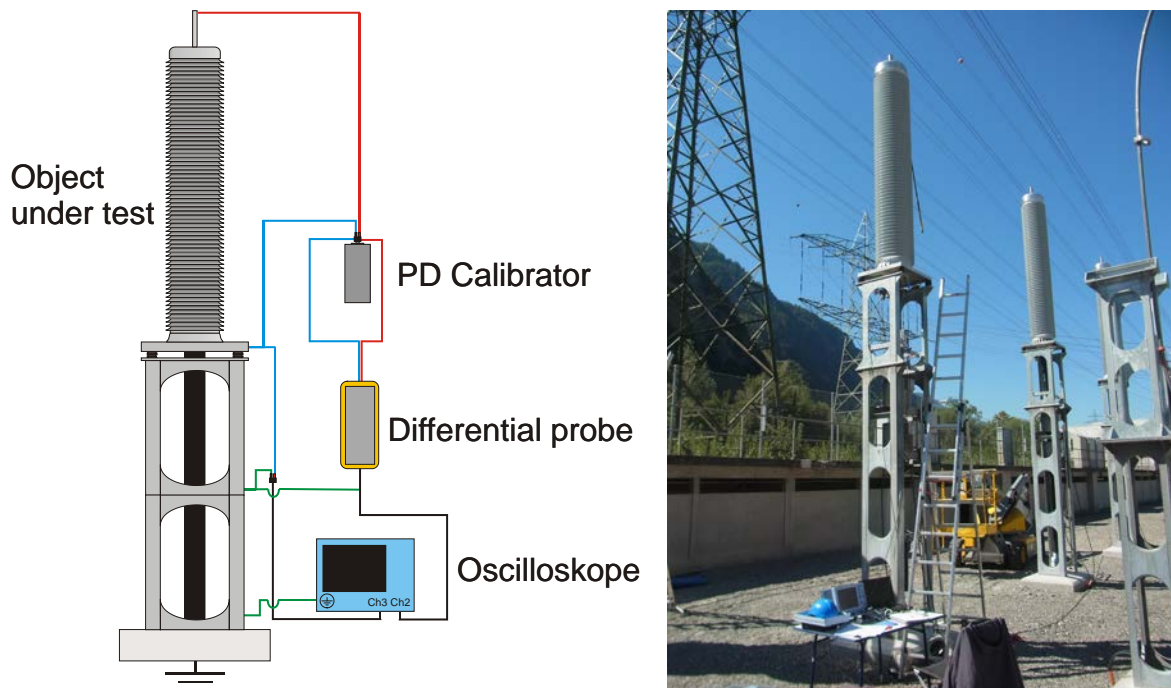


Figure 3-7: The on-site measurement setup without the HV installation

In the last case the separate cable termination was measured. Table 3-A presents all the measurement results. As expected, measurement sensitivity decreased, but also due to the extra stray inductances of the measurement cables, higher frequency oscillation appeared, as it can be seen on the 10 nC case. This caused the measurement being affected by external effects, e.g. the wind. This oscillation lead to useless measurement results in the 50 nC case. To mitigate this problem, additional grounding cables were added, as it can be seen on Figure 3-7.

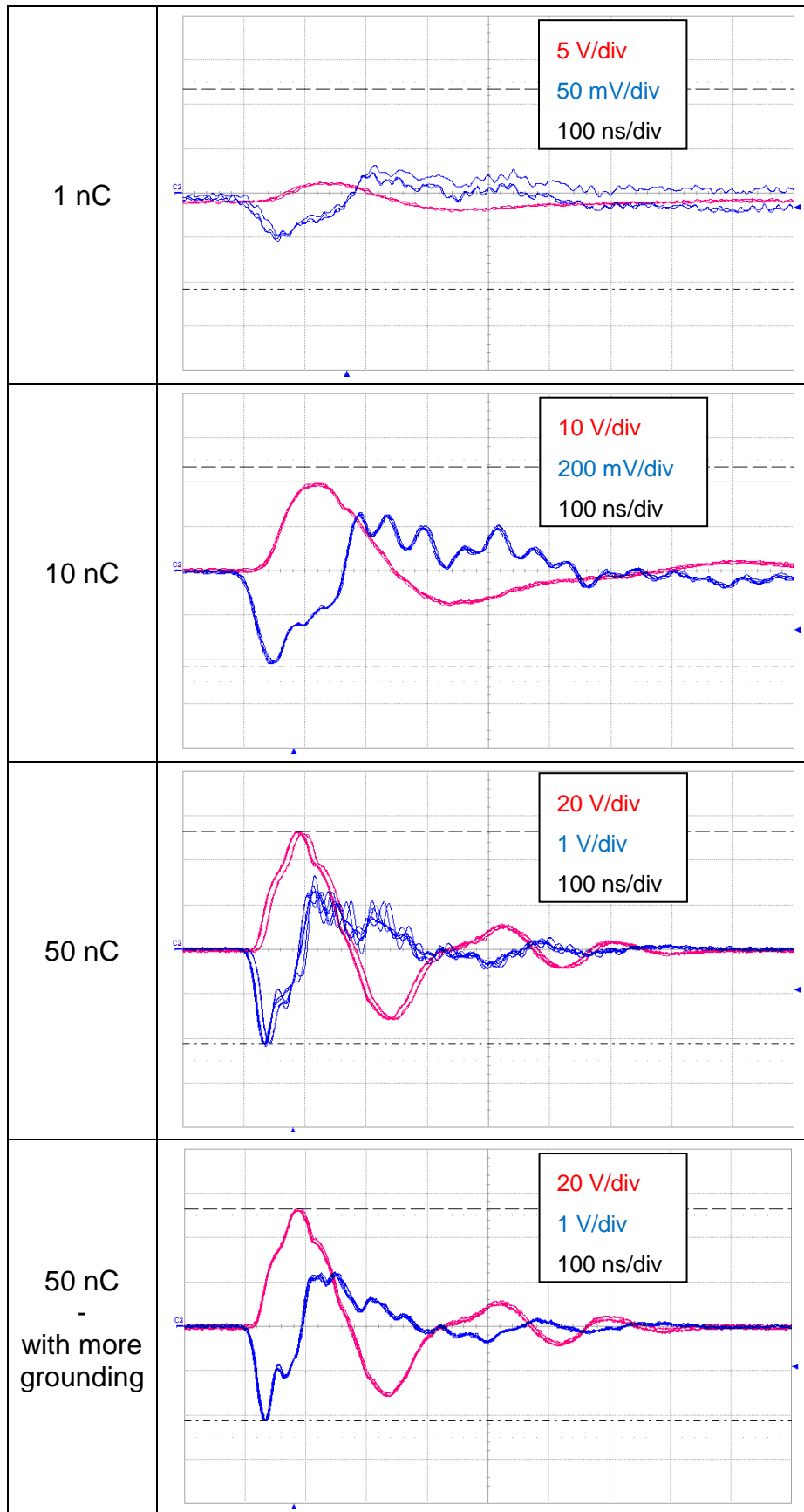


Table 3-A: Results of the on-site measurement with separate termination

Since the measurement setup was altered during the measurements (and due to the limited time frame there was no option to repeat the measurements), the data of the last measurement is going to be used for the simulations. Figure 3-8 shows the

calculated linearity of the measurement. It can be well seen, that despite the decreased sensitivity and lack of external capacitor, the voltage peak is still linearly dependent on the injected charge. It is a very promising result, because it means the measurement method has a sufficiently high signal to noise ratio that even without narrow or wide band filters.

It can also be noted, that the peak of the differential probe signal is not a linear function of the injected charge. This is due to the filtering characteristics of the probe. This problem is going to be discussed in detail in chapter 4.2.

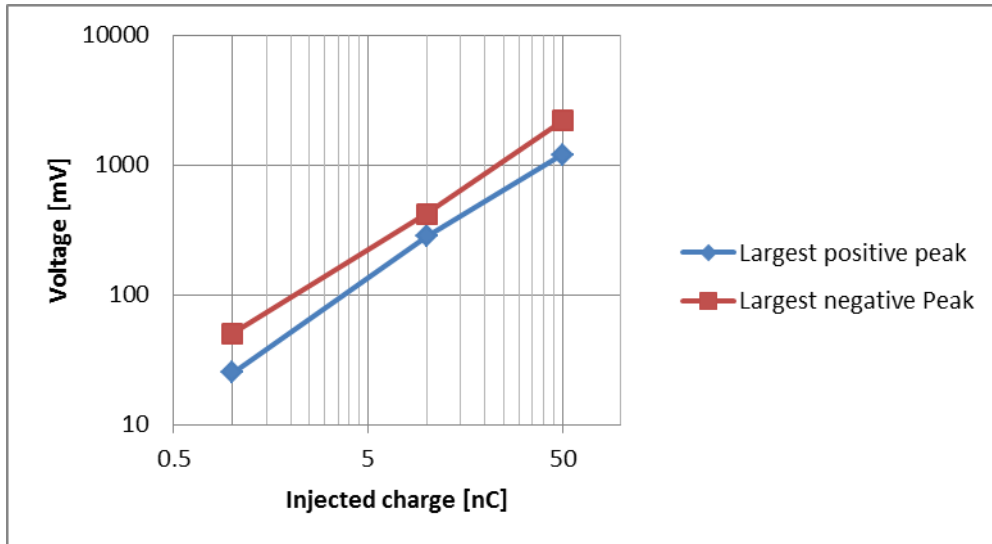


Figure 3-8: Linearity of the measurement results of the separate termination

4. Simulation in Micro-Cap

As we could see in the previous chapter, the measurements results suggest a highly linear response, thus a model using linear components is sufficient for the simulation. In this chapter I present the development of the PD calibrator model, the differential probe model and the model for the two measurement setups. The simulation results are compared to the measurement results and the validity of the models are tested. For all simulations Micro-Cap 9 was used.

4.1 PD Calibrators

As mentioned in chapter 2, the previous intern also pointed out that “One problem with the simulation is that the structure of the calibration equipment is not well known and thus it is impossible to build an accurate model for the calibrator. The structure of the Calibrator determines how the calibration pulse looks like and this has an effect on the simulation results” [6]. Therefore creating an exact calibrator model was a priority from the beginnings.

During the measurements two calibrator types were used; a Power Diagnostix Cal 1A (maximal injected charge: 100 pC) and Power Diagnostix Cal 1C (maximal injected charge: 50 nC). The basic work principle of these calibrators is that there is a voltage source connected in series with a small capacitance (C). As it is well known, when a voltage step (U) appears on the source, then a very well defined, exponentially decreasing current runs through the system. The charge (Q) is the time integral of this current, which can be easily calculated using $Q=C*U$.

Unfortunately, the real calibrator is far from the ideal case described above. Figure 4-1 shows that in reality a negative overshoot can be observed on the oscilloscope. To minimise the external noise, direct BNC connection was made between the PD calibrator and the Oscilloscope, as it can be seen on Figure 4-2.

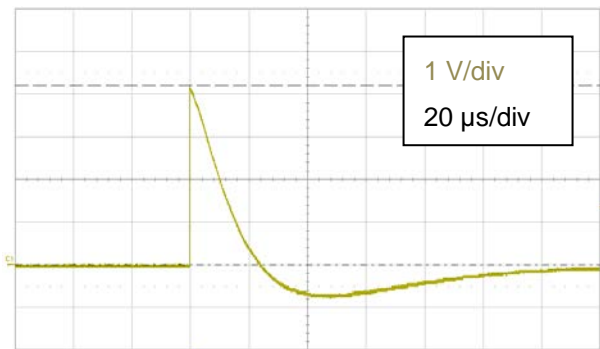


Figure 4-1: Oscillograph of the real PD calibrator

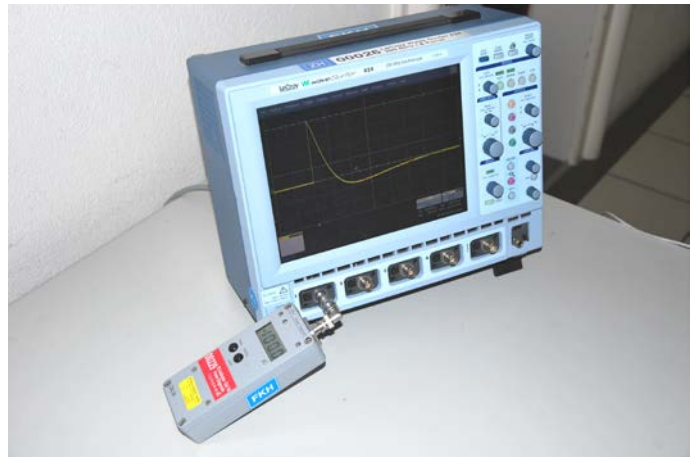


Figure 4-2: Setup of the calibrator measurement

To oscilloscope's input impedance was set to be 1 M Ω , in this case the stray capacitance is 16 pF. To rule out the possibility, that the negative overshoot presented on the oscilloscope was due to the internal circuit, an ideal PD source was also created. The setup of the ideal calibrator can be seen on Figure 4-4. It is consisted of a signal source with a voltage step of 10 V and an approximately 10 pF capacitance soldered into a small coaxial fixture case (Sucobox).

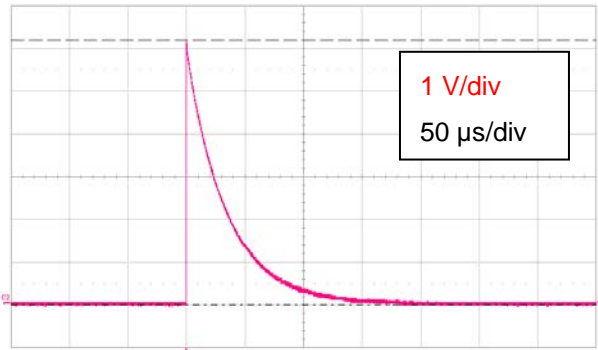


Figure 4-3: Oscilloscope of the ideal PD calibrator composed of an impulse generator –capacitor combination

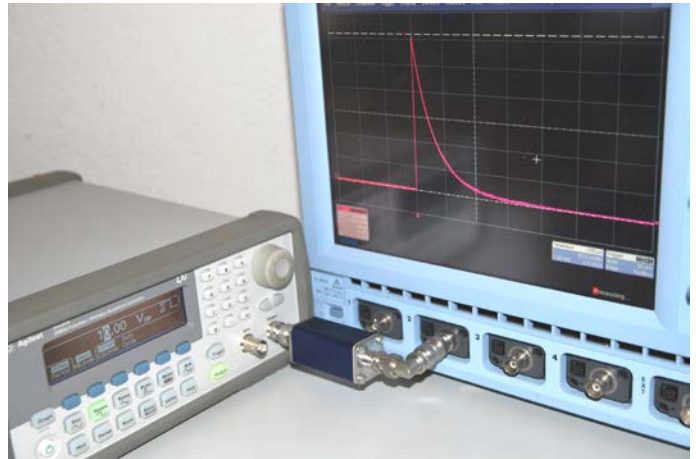


Figure 4-4: Setup of the custom-made calibrator measurement

Figure 4-3 shows the resulting waveform. As expected there is no swinging, which means the negative overshoot is due to the calibrator and it must be modelled. The option was also considered not to use the Power Diagnostix calibrator, because such a custom-made calibrator is much more reliable. This option was eventually abandoned due to the employer's direct request.

4.1.1 Power Diagnostix CAL1A calibrator

To produce the required swinging, a more complicated model is necessary. Firstly, an obvious idea for a modification was investigated: adding a series inductance to the circuit. Unfortunately this circuit does not result in a similar waveform, like on Figure 4-1, even not after multiple parameter variations. The negative overshoot can be modelled by adding a 40 H parallel inductance to the circuit, but this solution is not based on the physical realities.

A different approach was used to model the negative overshoot: an additional RC part was added to the circuit, as it can be seen on Figure 4-5. It consists of a voltage source, the additional RC part, our original series capacitance and the measuring impedance with the stray capacitances. The principle considers that at the moment of the voltage step, the resistances can be neglected and the voltage is divided through the capacitances. Thereafter the C1 capacitance is charged by the source, the other capacitances are discharged through the resistances.

With the correct parameters this circuit can produce the wanted waveform as it can be seen on Figure 4-6. As we mentioned earlier the measuring resistance of the oscilloscope is 1MΩ with 16 pF stray capacitance. The BNC connectors also have an additional 10 pF capacitance. We also know from the datasheet of the calibrators [7], that the inner capacitance of the CAL1A calibrator is smaller than 1 pF. That means we need a 100 V voltage step to produce a charge of 100 pC. The step-up time was successively measured to be 16 ns, using linear extrapolation based on the voltage values at 10% and 90%. It must also be noted that the PD calibrator is able to produce positive and negative discharges. The explanation to that is that the voltage step is actually a voltage ramp with a repetition period of 20 ms.

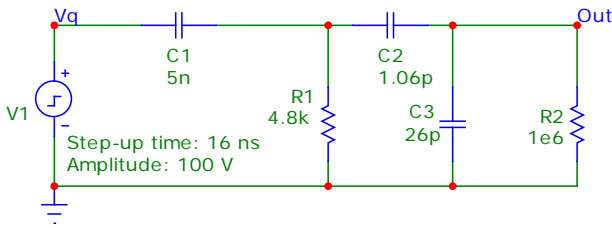


Figure 4-5: Circuit diagram of the developed PD calibrator model

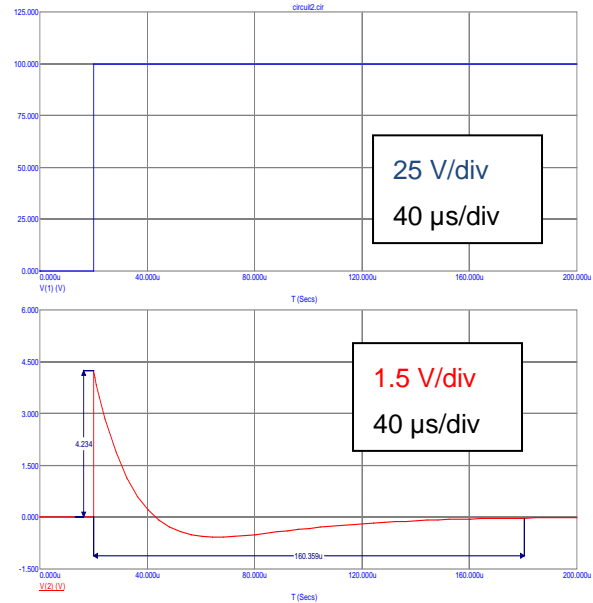


Figure 4-6: Waveform of the developed PD calibrator model

The remaining missing parameters (namely C1, C2 and R1) can be freely chosen to produce the required output. To find the correct values, a series of experiment was conducted by connecting different loads between the calibrator and the oscilloscope, like on Figure 4-8. The loads always consisted of a parallel resistor and a parallel capacitor soldered into a sucobox as it can be seen on Figure 4-7. The missing parameters were chosen so that the resulting waveforms are as close to the measured waveforms as possible. The summary of the various measurements and the comparison with the model is to see in appendix III.

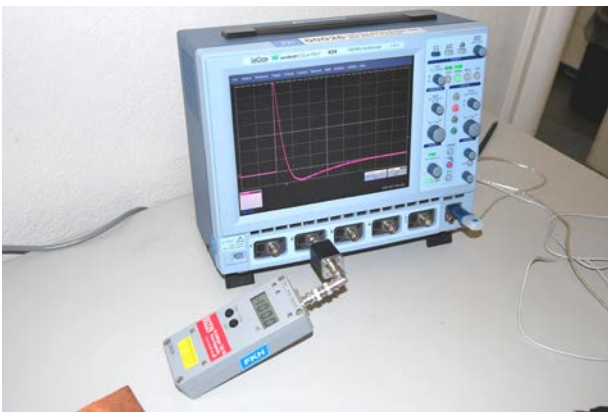


Figure 4-7: Measurement setup of the load variations to the CAL1A calibrator

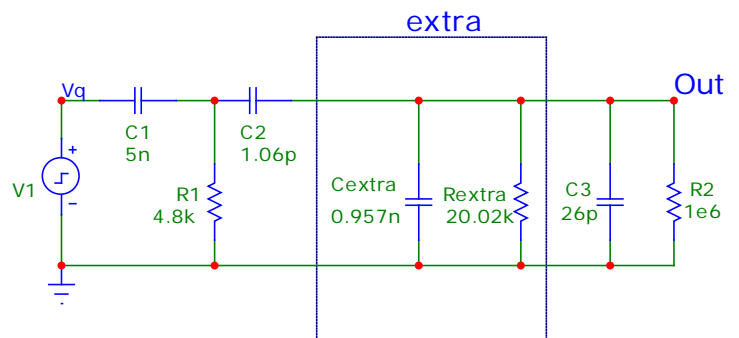


Figure 4-8: Circuit diagram of the load variations to the CAL1A calibrator

Since during the measurement a large inductance is present in the circuit, the PD calibrator model was also briefly investigated using an inductive load. The results were adequate, but it must be mentioned that the high frequency behaviour of the used inductance coils were not well known.

One unfortunate consequence of the developed calibrator circuit, that the injected charge cannot be determined so easily like in the ideal case. Using notations from Figure 4-8, it can be also noted that the injected charge is dependent on the size of the external resistance (R2). Since the capacitances are discharging also through the internal resistance (R1) and also through the external resistance, if the external resistance is too high, only a small portion of charge is flowing through it. (The measurement data is supporting this idea, since the measured voltage signal (Figure

4-1) divided by the measuring resistance and integrated has a maximum value of only 40 pC.) Equation 4-1 presents an approximation for calculating the injected charge. If we suppose the load is much smaller than the internal resistance (which is the case in practical applications), the internal resistance can be neglected. Thus the injected charge can be easily calculated by $Q=C' \cdot U$, where C' is the series equivalent of the C_1 and C_2 capacitances. In the case of the CAL1A calibrator C' is 1.059 pF (just as we expected from the datasheet [7]) and thus the injected charge is 106 pC.

$$Q = \int_0^{\infty} i_R(t) dt = \frac{C_1 * C_2}{C_1 + C_2} * V_1 = C' * V_1$$

Equation 4-1 Approximation for calculating the injected charge by the calibrator

As it can be concluded from appendix III, the created calibrator model is matching the measurement results fairly well, and the calculated injected charge also fits the requirements.

4.1.2 Power Diagnostix CAL1E calibrator

As I mentioned in chapter 3.2, due to the high background noise, another PD calibrator had to be used during the on-site measurement. The circuit, which was detailed in the previous chapter and proved to be modelling the CAL1A calibrator very well, is unfortunately not satisfactory in this case. After unsuccessfully attempting to find the parameters following the same method as in the previous chapter, I took a new approach by calculating the differential equations of the voltage response.

The CAL1E calibrator has an internal capacitance (C') smaller than 500 pF according to [7]. The step-up time was successively measured to be 12 ns. All measurements were conducted using the 10 nC level. The model was defined using three measurement layouts. In the first case (A) there were no extra load between the calibrator and the oscilloscope. In case (B) a parallel capacitance ($C_{extra}=1nF$), in case (C) a parallel resistance ($R_{extra}=100 \Omega$) was connected between them. (Notations are still based on Figure 4-8.) Appendix IV presents the measurement results and the results of two unsuccessful parameter variations.

A series of differential equations were calculated to determine the voltage output of the different measurement setups. Equation 4-2 (A) is the formula for the voltage response, when there is no additional load in the system. It was calculated neglecting the R_1 resistance and the step-up time. Based on the measurement the peak value should be 20.6 V. Equation 4-2 (B) was calculated in the same fashion for the case (B). Equation 4-2 (C) is different, since the R_{extra} , shunt resistance is so small, that the step-up time cannot be neglected. Therefore it was calculated using the integral of the solution to the step-up function. All three equations were verified by comparing with data simulated in Micro-Cap and the difference was smaller than 0.1%.

$$\begin{aligned} (A) \quad v_o &= V_1 * \frac{C'}{C' + C_3} * e^{-\frac{t}{R_2 * (C' + C_3)}} = 20.6 V \\ (B) \quad v_o &= V_1 * \frac{C'}{C' + C_3 + C_{extra}} * e^{-\frac{t}{R_2 * (C' + C_3 + C_{extra})}} = 7.4 V \\ (C) \quad v_o &= \frac{V_1}{t_{step-up}} * C' * R_{extra} \left(1 - e^{-\frac{t}{R_2 * (C' + C_3)}} \right) = 11 V \end{aligned}$$

Equation 4-2: Simultaneous equations describing the voltage output of the three different cases

Once the equation system is defined we can calculate the values of C1, C2 and V1. Since R1 has no influence on the maximal value, it can be used to adjust the slope of the function. Using the solver function of MS Excel these values were calculated to match the measurement data. There were also two conditions: $C' \leq 500$ pF and $Q = 10$ nC. Table 4-A presents the calculation results. These parameters are unsatisfactory, since with low ohmic load, the model deviation is above 140%.

C1=	2150	pF	V _{0A} =	17.42	V
C2=	651.5	pF	V _{0B} =	6.01	V
V1=	18.3	V	V _{0C} =	15.58	V
C'=	500	pF	Q=	9.17	nC

Table 4-A: Result of parameter variation using the same RMS weighting

There were also numerous attempts to develop this model by adding additional RC parts, not neglecting the R1 terms, returning to the model with inductance and also by neglecting the negative overshoot. Unfortunately none of these resulted in a better solution. Eventually a compromise was made to have calibrator model response correctly to low ohmic loads, because it was the case at the on-site measurement. Therefore the Equation 4-2 was used again with a weighting forcing Q and V_{0C} to match better the measurement results. Table 4-B presents the applied values, Figure 4-9 is the circuit diagram of the final PD calibrator model.

C1=	1509	pF	v _{0A} =	15.32	V
C2=	966.5	pF	v _{0B} =	5.84	V
V1=	16.0	V	v _{0C} =	13.92	V
C'=	589	pF	Q=	9.43	nC

Table 4-B: Result of parameter variation using uneven RMS weighting

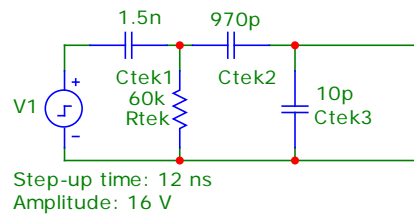


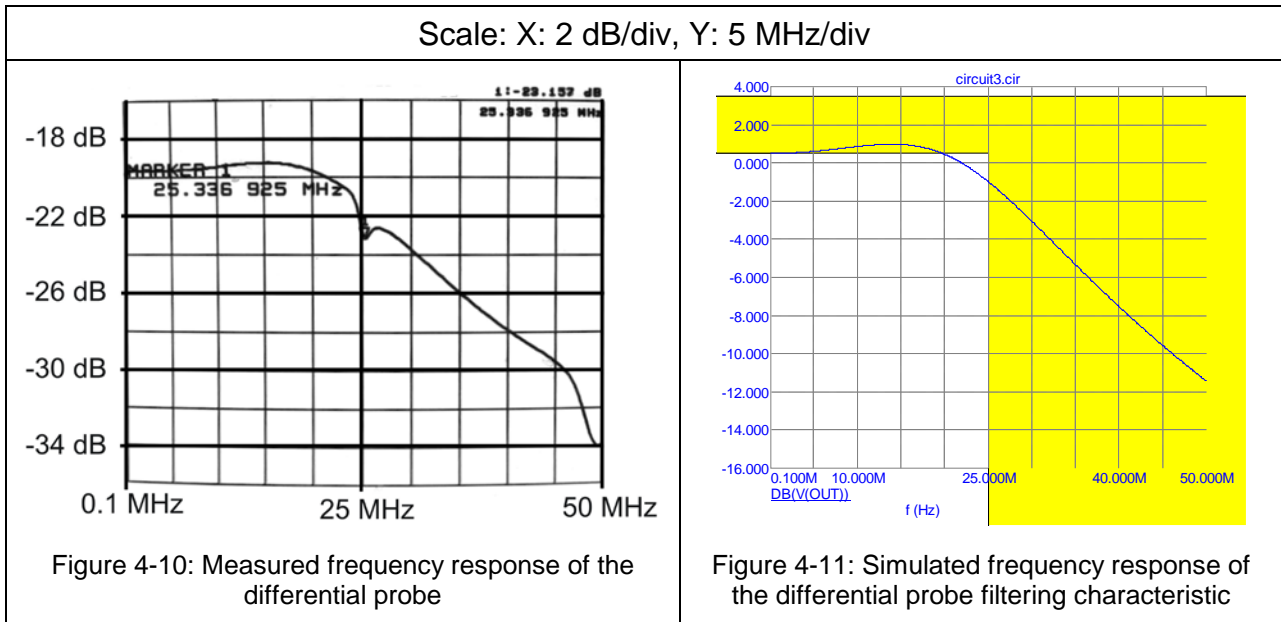
Figure 4-9: the final CAL1E PD calibrator model

4.2 TT-SI 9001 Differential probe

The differential probe is not an essential part of the measurement setup, but a valuable source of additional information, which may be well used for model validation. The used differential probe has a 4 MΩ input impedance and a rise time of 14 ns. It has two attenuation levels, but 1:10 attenuation ratio was applied for all measurements. According to the datasheet both test leads have 5.5 pF capacitance to ground. The complete datasheet of the differential probe can be seen in appendix V.

There was also an additional 12 pF capacitance measured between the two cables. This capacitance in reality appears as 10 pF only, since the aforementioned two 5.5 pF capacitance appears as parallel coupling during the measurement.

The datasheet informs us, that the -6 dB cut-off frequency is at 25 MHz. As we could see in chapter 3, the measurement results often fall into this frequency domain, therefore a more subtle investigation is required. Therefore the exact frequency response of the differential probe was measured; the results are presented on Figure 4-10. The measurement procedure is not going to be detailed here.



It can be recognized, that the probe is indeed -20 dB attenuated in the 0.1-20 MHz domain. There is a definite valley at 25.3 MHz with -23 dB and from then it is in the cut-off region. Using Micro-Cap a simple stage Chebyshev Sallen-key low-pass filter was designed using an ideal op-amp. For the simplicity of the calculation the 1:10 attenuation was simulated by dividing the signal, and the filter model was used to simulate the nonlinearity of the probe. The frequency response of the filter model can be seen on Figure 4-11. Please note that the local minimum at 25.3 MHz is not simulated.

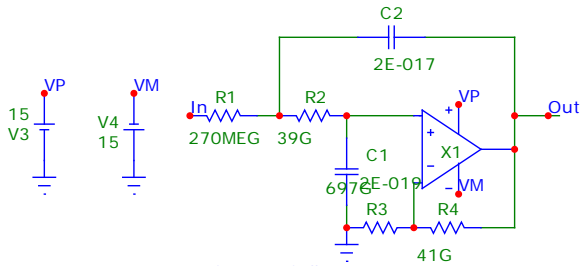


Figure 4-12: Circuit model of the active low-pass filter

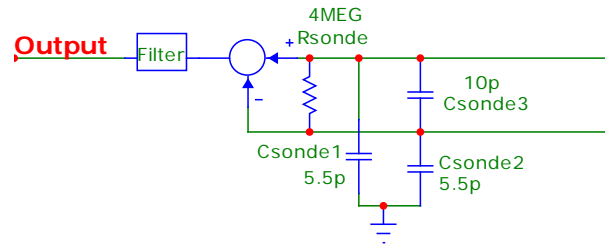


Figure 4-13: The final differential probe model

Figure 4-13 shows the final differential probe model. For simplicity the filter model was stored in a macro, and it was simply represented by a box in the probe model. As a summary the model of the differential probe matches the measured frequency response very well, the stray capacitances - even though they are relatively small and negligible - are still to be verified.

4.3 Model for the laboratory measurement

This chapter is going to detail the simulation of the laboratory test setup. As mentioned earlier, the previous intern also noted that “it is almost impossible to get the simulation results to match the laboratory measurements. [...] The inductances were near the low end limit of the inductance measurement equipment. Thus the inductance measurement was not that accurate.” [6] Measuring the stray capacitances was also a big challenge, since the layout of the measuring equipment also had a great influence on the results.

Due to all these uncertainties, the aim of the measurement was to determine the domain of values as accurately as possible. The actual values are going to be derived from parameter variations of the measured model.

4.3.1 Definition of inductances

Inductance in the model is represented by two loops. Firstly there is the inductance of the calibrator cable-cable core loop but we must note that there is also another loop. This second loop is due to the fact that our signal is travelling through stray capacitances, therefore this second loop also has to have some capacitance. Since all other cables were made as short, as possible, all other inductances were neglected.

Figure 4-14 represents the measurement setup of the loop measurement. Note that during the actual measurement, the differential probe cables were not connected. The BNC connector between the cable core and the cable shielding (metal plate in this case) was short-circuited. The RLC meter was positioned in a way that the measuring cable is in the same position as when the PD calibrator is connected. The RLC meter was calibrated by connecting a very short cable between the two terminals. The measurement result is 1.9 μH .

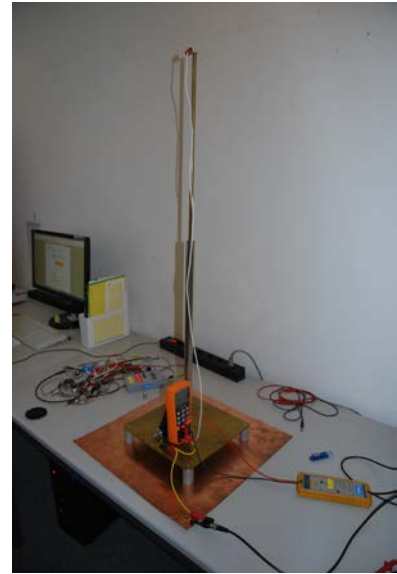


Figure 4-14: Inductance measurement setup of the calibration cable-cable core loop

As a reality check an approximate calculation was also made, based on the formula for parallel cylindrical conductors. [8] The calculated value is 1.78 μH .

This value is the inductance that the calibrator “sees”. Since our signal is travelling through stray capacitances, this secondary, capacitive loop also has some inductance. Therefore the measured value must be split up between the calibration cable and the cable core. Using the approximation that every meter of a cable has about one μH inductance, the capacitive loop inductance was made to be **0.4 μH** and the measuring loop was made to be **1.4 μH** .

4.3.2 Definition of resistances

The two most dominant resistances of the model are the measuring resistance of the oscilloscope and the resistance connected between the cable core and the shielding plate. The latter is modelling a **50 Ω** characteristic impedance of an infinitely long cable connected to the cable termination. The input impedance of the oscilloscope was also set to be **50 Ω** and there is no stray capacitance in this case, since the characteristic impedance of the measuring cable already includes that. These two are high precision resistances, proved to maintain their values even in the operating region of 20 MHz.

Since our main harmonic lies in the MHz domain, it was a question whether the skin effect has a considerable influence on our signal form. Therefore based on [9], a series of calculation was conducted as it can be seen on Equation 4-3. (A) shows the value of skin depth for Brass, it was compared and verified by online values [10]. Equation 4-3 (B) presents the calculated value for the cable core resistance (value measured at 100 kHz is 30 mΩ), (C) shows the calculation for the measuring cable resistance (measured value is 73 mΩ at 100 kHz.).

$$(A) \delta = \sqrt{\frac{2}{\omega \mu_0 \mu_r \kappa}} = \sqrt{\frac{2}{2\pi * 20 \text{ MHz} * 4\pi * 10^{-7} * 1.427 * 10^7}} = 29.8 \mu\text{m}$$

$$(B) R_{\text{cable core}} = \frac{l}{\kappa \delta D \pi} = \frac{l}{1.427 * 10^7 * 29.8 \mu\text{m} * 1 \text{ cm} * \pi} = 75.6 \text{ m}\Omega$$

$$(C) R_{\text{cable}} = \frac{l}{\kappa \pi (\delta D - \delta^2) N} = \frac{1.08 \text{ m}}{1.427 * 10^7 * \pi * (29.8 \mu\text{m} * 0.2 \text{ mm} - (29.8 \mu\text{m})^2) * 30} = 158 \text{ m}\Omega$$

Equation 4-3: (A) Formula for penetration depth of brass (B) Formula for the resistance of the cable core considering skin effect, (C) Formula for the resistance of the measuring cable considering skin effect

It can be concluded, that the increased resistance values are still negligible compared to the resistance of the oscilloscope and the characteristic impedance. Therefore these calculations are going to be neglected at the construction of the on-site measurement simulation.

4.3.3 Definition of stray capacitances

The measurement of the capacitances was the most delicate measurement process, which was repeated multiple times. During these measurements the BNC connector between the cable core and the shielding plate was removed, leaving the two open circuited. The calibration was done by connecting the brown measuring cable to the RLC meter, but not connecting to the ground plate. The white measuring cable (which is the same used to connect the PD calibrator to the cable core) was not connected during calibration, as it can be seen on Figure 4-15. The reason for not connecting is that the white calibration cable also has a great capacitance to ground. Figure 4-16 shows the actual measurement setup. All measurements were repeated twice, the calibration was conducted in both cases. The averaged value of measurements is the following: $C_{\text{Ground-Shielding}}=41.3 \text{ pF}$, $C_{\text{Shielding-Core}}=70.8 \text{ pF}$ and $C_{\text{Core-Ground}}=31,5 \text{ pF}$.



Figure 4-15: Calibration setup for the $C_{\text{Core-Ground}}$ measurement



Figure 4-16: Measurement setup for the $C_{\text{Core-Ground}}$ measurement

The measured capacitances are not the resulting capacitances, because during every measurement the actual capacitance is coupled by the series equivalent of the other two capacitances. To get the resulting capacitances, the following equation system must be solved:

$$C_{\text{Ground-Shielding}} = C_1 + \frac{C_2 C_3}{C_2 + C_3}$$

$$C_{\text{Shielding-Core}} = C_2 + \frac{C_1 C_3}{C_1 + C_3}$$

$$C_{\text{Core-Ground}} = C_3 + \frac{C_1 C_2}{C_1 + C_2}$$

Equation 4-4: Simultaneous equations describing the relation of the measured capacitances and the resulting capacitances

The solution is **C1=32.5 pF**, **C2=63.1 pF** and **C3=10 pF**. All other stray capacitances were neglected in this model.

4.3.4 Parameter fine-tuning

As it was emphasised above, the measurements are suitable to find the magnitude of the parameters, but not to determine the exact values. Figure 4-17 presents the complete circuit diagram of the laboratory measurement model, based on previous sections. The cable core is represented by a vertical box containing the capacitive loop inductance and the calculated resistance of the core. The shielding and the ground are two vertical boxes. The calculated capacitance values are connected between them. The PD calibrator is connected between the shielding and the core, the oscilloscope between ground and shielding. The coax cable connecting the oscilloscope can be neglected, since it is coupled by its characteristic impedance, 50 Ω.

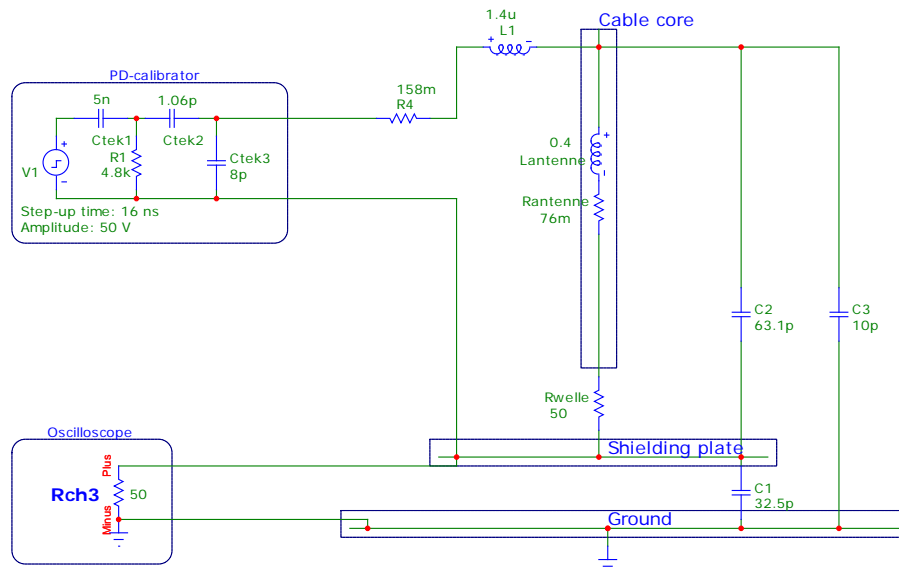


Figure 4-17: Circuit diagram of the laboratory setup - based on measured values

Figure 4-18 shows on the left side the measurement data (same as Figure 3-2), on the right side the simulated waveform based on the circuitry above. The most obvious conclusion is that the amplitude of the waveform is too small. The attenuation also differs, but it is not due to the resistance values. It can be noted, that the angular frequency is also smaller, thus the inductances must be greater and the capacitances smaller.

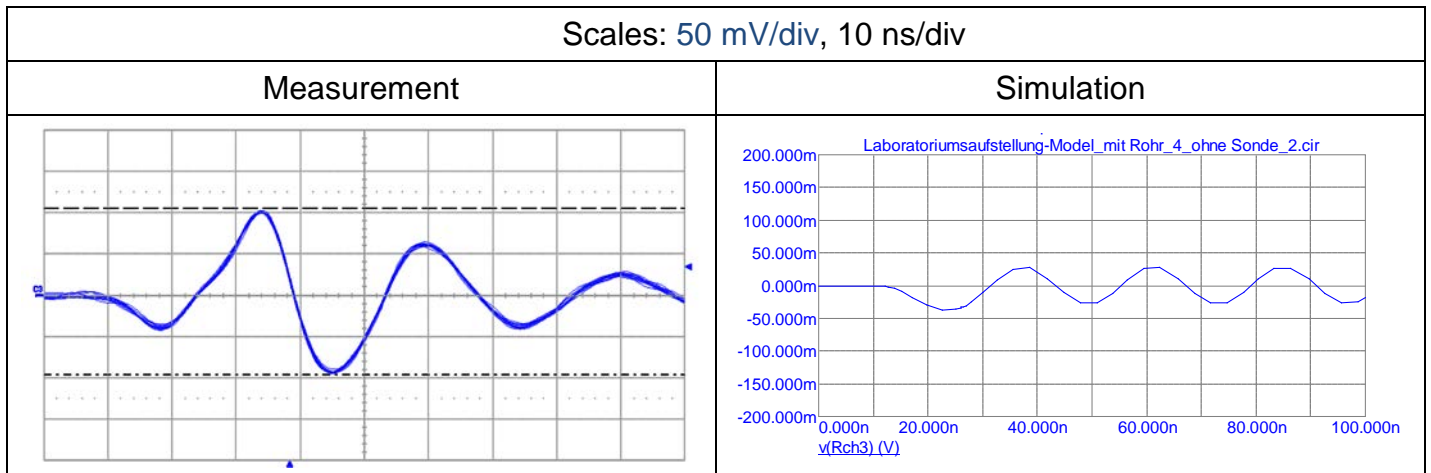


Figure 4-18: Comparison of measurement and simulation results - based on the measured parameters

The parameter fine-tuning was done using the Optimization module of the Micro-Cap. Here it is possible to define limits to the parameter and define conditions for the result. In this case conditions were set to match the peaks and valleys of the waveform and to match the angular frequency. Appendix VI presents some key steps in the tuning process. It must be noted, that the plausibility of the parameters were considered more important, than the similarity of the waveforms.

Figure 4-19 shows the result of parameter variations on the same circuit diagram. As a summary it can be noted that the inductance was indeed proved to be greater, the capacitances smaller than on the measurement. It can be also seen, that relatively minor changes were made in comparison with the measured data.

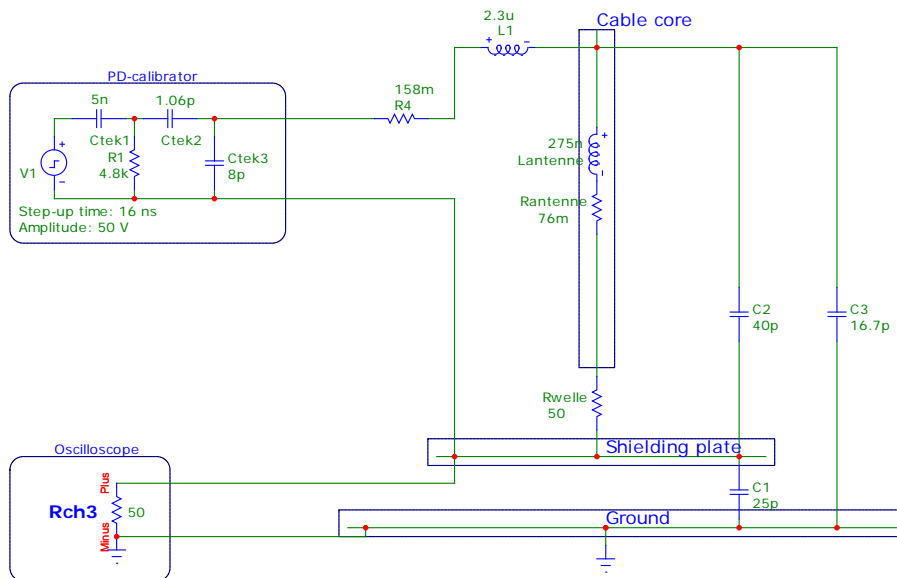


Figure 4-19: Circuit diagram of the laboratory setup - after parameter variation

The final result of the parameter fine-tuning can be seen on Figure 4-20, on two different time-scales. It can be concluded that the parameter variation was successful, the deviation of parameters is plausible and the model is matching the laboratory setup considerably well.

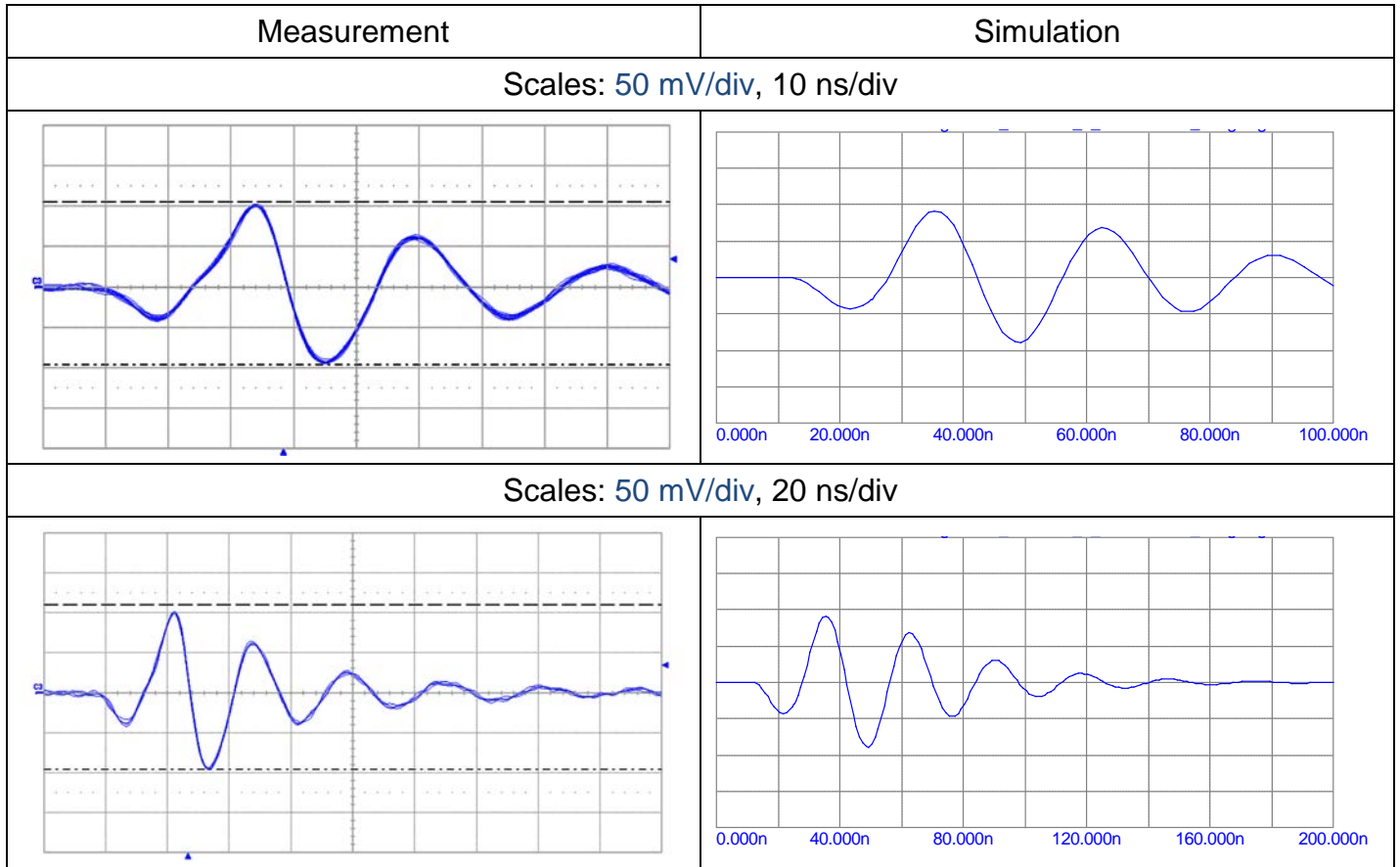


Figure 4-20: Comparison of measurement and simulation results - after parameter variation

4.3.5 Comparison of measurement and simulation results

It is easy to recognise that the model is also matching the other measurement data as well, since we could see the linearity of the model in chapter 3.1.3. The model is going to be verified in this chapter using two different approaches.

4.3.5.1 Comparison in frequency domain

Using the same frequency analyser as with the differential probe, the frequency response of the laboratory setup was measured. For the test purposes the PD calibrator was removed and the voltage input was placed between the cable core and the ground, the voltage output was connected in place of the oscilloscope; between the shielding plate and the ground. Figure 4-21 shows the measurement results, Figure 4-22 shows the simulation results. It can be seen that the two responses are quite similar in trend, but the simulation tend to be steeper. It is particularly convincing evidence, since even though different input and outputs were chosen, the model reacted correctly.

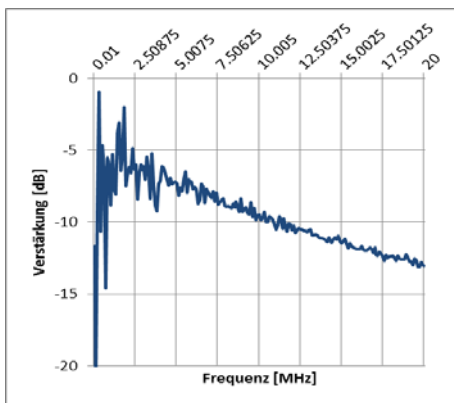


Figure 4-21: The measured frequency response of the laboratory test setup

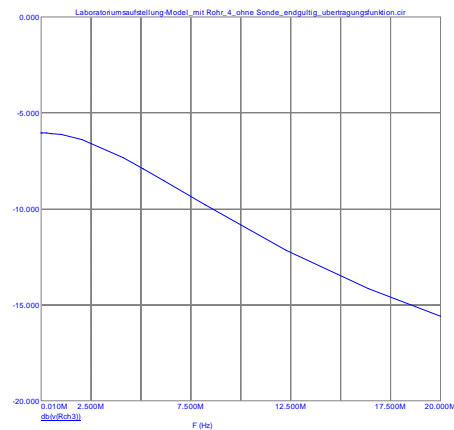


Figure 4-22: The simulated frequency response of the laboratory test setup

4.3.5.2 Comparison with differential probe

To gain additional information for the validation of the model, the differential probe was connected to the output of the PD calibrator, as it can be seen on Figure 4-23. Figure 4-24 shows the circuit model extended with the probe.

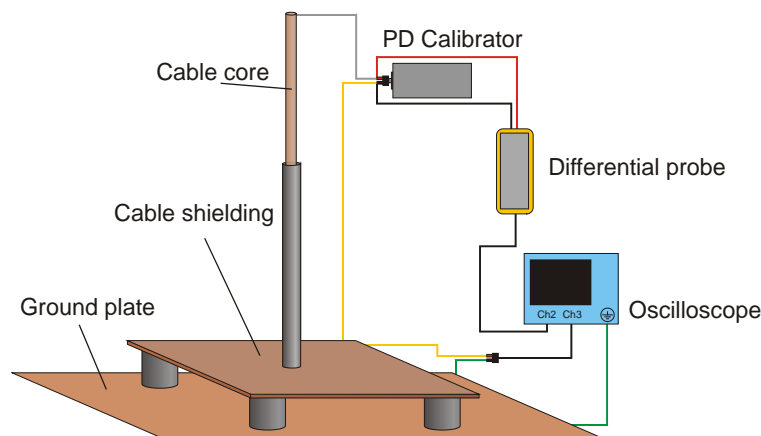


Figure 4-23: Laboratory test setup extended with the differential probe

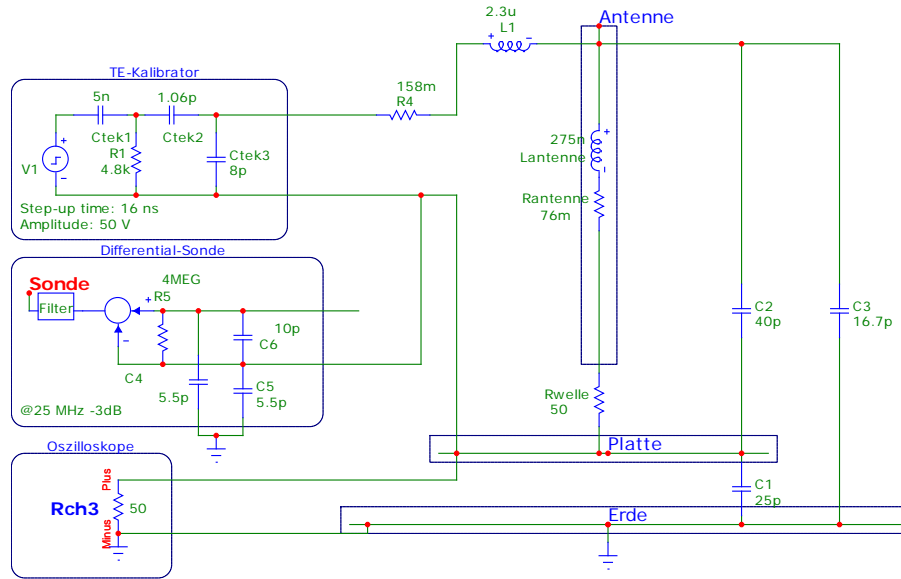


Figure 4-24: The laboratory circuit extended with the differential probe model

To investigate the effect of the differential probe to the model, different connections were made. First only the positive test lead was connected, then only the negative lead, then both. Table 4-C shows the comparison for the three cases. For better comparison both diagrams use the same scaling.

Scales: 50 mV/div, 200 mV/div, 20 ns/div		
	Measurement	Simulation
Only negative test lead		
Only positive test lead		
Both leads are connected		

Table 4-C: Comparison of measurement and simulation data on the laboratory setup with differential probe

It can be seen that the signal between the ground and shielding plate is reacting very well for the new input. It must be noted though, that the deviation of the differential probe model becomes considerable, when the oscillation falls in to the 24-28 MHz domain. As it was detailed on Figure 4-10 and Figure 4-11, the differential probe model does not have that particular valley at 25 MHz. This means, that when the oscillation of the signal is around 25 MHz the simulation is representing higher amplitude, than what can be seen in reality.

4.4 Model for the on-site measurements

In the case of the on-site measurement it is not possible to measure the various parameters of the cable termination with RLC meters. These parameters were determined using theoretical approximations and linear scaling based on the experiences from the laboratory model. The blueprint of the cable termination can be seen on Appendix VII, the datasheet of a HV cable with similar configuration can be seen on Appendix VIII.

4.4.1 Definition of inductances

In the case of the on-site measurement two different inductances had to be calculated. Firstly the same cable core-calibrator cable loop as in the case of the laboratory model, secondly the inductance of the measurement cable.

The cable core, with the calibration cable forms a big loop in a similar fashion like at the laboratory model. Using the same parallel cylindrical conductor formula [8] as in the previous case, the inductance of the loop is calculated to be $5.56 \mu\text{H}$. Based on the experience from the laboratory measurement, the actual value of the inductance is tend to be higher, than the calculated value. Using the proportion gained from the laboratory model ($2 \mu\text{H} / 1.78 \mu\text{H}$), the actual inductance value is calculated to be about **$6.25 \mu\text{H}$** . Based on the length of the cable core, the inductance of the capacitive loop is estimated to be **$3.3 \mu\text{H}$** .

The other considerable inductance is of the cable shown on Figure 4-25. It must be considered in the simulation, because a too long cable was used between the shielding and the coaxial cable of the oscilloscope. It is a particularly important mistake, since this inductance appears as high impedance to our high frequency signal. The value of inductance was estimated from two directions. The high estimate was based on the formula for inductance of parallel cylindrical conductors, the low estimate was based on the formula for coaxial cables [8]. The first resulted $1.72 \mu\text{H}$, the latter resulted $1.11 \mu\text{H}$, thus the estimated value is set to be **$1.4 \mu\text{H}$** .

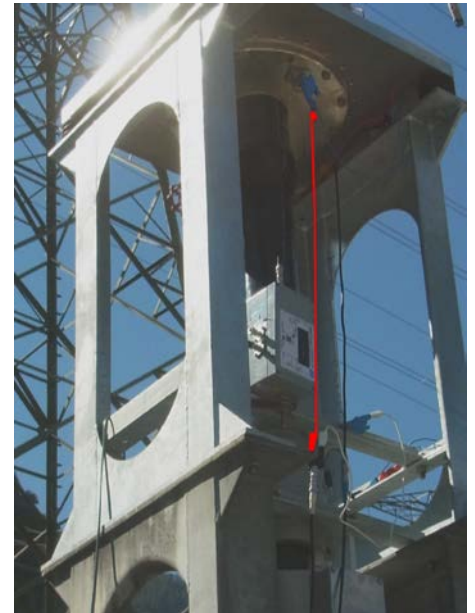


Figure 4-25: Position of the measurement cable (marked with red) connecting the shielding plate to the coaxial cable

4.4.2 Definition of resistances

The measuring impedance of the oscilloscope is again **50Ω** . The characteristic impedance of the cable was derived to be **55Ω** from the datasheet of a similar cable (appendix VIII) using linear extrapolation. Even though the cable is not coupled by the characteristic impedance, it is not necessary to model the reflections. The length of the cable is 430 m, thus the delay of the reflection is approximately $2.8 \mu\text{s}$, which is far behind the observed region. As described in the case of the laboratory model (chapter 4.3.2), the skin effect does not have a considerable effect in this frequency domain.

4.4.3 Definition of stray capacitances

Compared to the laboratory model, the capacitance calculation is much more complicated in this case. Previously we had to consider only three different capacitances (ground-shielding, shielding-core, core-ground). In this case we also have to consider the effect of the stress cone (chapter 4.4.4) and the effect of the cable shielding (chapter 4.4.5). In addition to this, the cable core was divided into three segments, so that the effect of stray capacitances can be modelled more precisely. In this case no on-site measurement is possible, thus approximate calculations were used based on [11].

The most significant capacitance, the ground-core capacitance was calculated to be 37 pF. If the core is divided to three equal parts, then the capacitance values are **16.3 pF**, **16.3 pF** and **16.2 pF**. (The similarity is due to the relative great distance to the ground.)

4.4.4 Definition of the stress cone model

The greatest capacitance between the cable core and the shielding is the stress cone. It is modelled following the norms using a capacitance and an RC part as it can be seen on Figure 4-26. As expected this model behaves like an open circuit to high frequency signals, thus it has no effect on our signal.

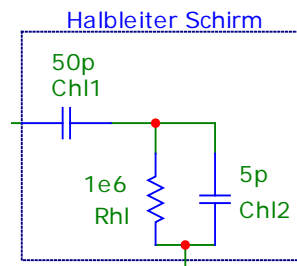


Figure 4-26: The stress cone model

There is also a smaller capacitance between the core and the shielding; the stray capacitance of the plate. It was also calculated to be around 15 pF, and it was divided to **8 pF**, **2 pF** and **2 pF**.

4.4.5 Definition of cable shielding model

The capacitance between the ground and the shielding is the most complicated part of the whole model. The shielding is separated from the earth by a relatively thin insulator, which runs 430 m long. This suggests a high capacitance value, some inductance and a spreading resistance too. The proper definition of the model would require long simulations using finite element method, thus due to limited timeframe just an approximate model was used. Figure 4-27 shows the cross-section of the cable. The resistance between the core and the shielding is the above described 55 Ω wave impedance of the cable. The cable core was modelled by an RL part with capacitances distributed between them. It is difficult to say any order of magnitude to the parameters, but eventually the resistance was chosen to be **300 Ω** , the inductance **10 μH** , C_{shield} **1 nF** and C_1 **200 pF**.

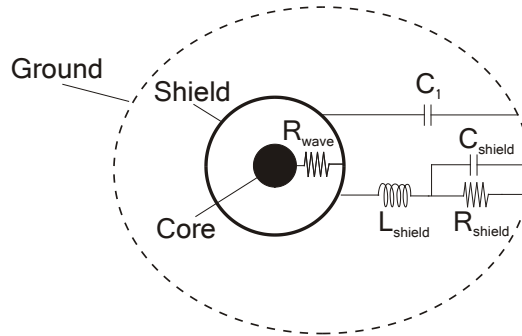


Figure 4-27: Approximate model of the cable shielding

4.4.6 Parameter fine-tuning

The conclusion of the previous chapters can be seen on Figure 4-28. The rectangles mark the position of the ground, the shielding plate and the cable core. The latter was divided into three segments, the respective stray capacitances are connected to the different segments. It must be emphasised again, that these calculations are just estimations intended to represent the value's order of magnitude.

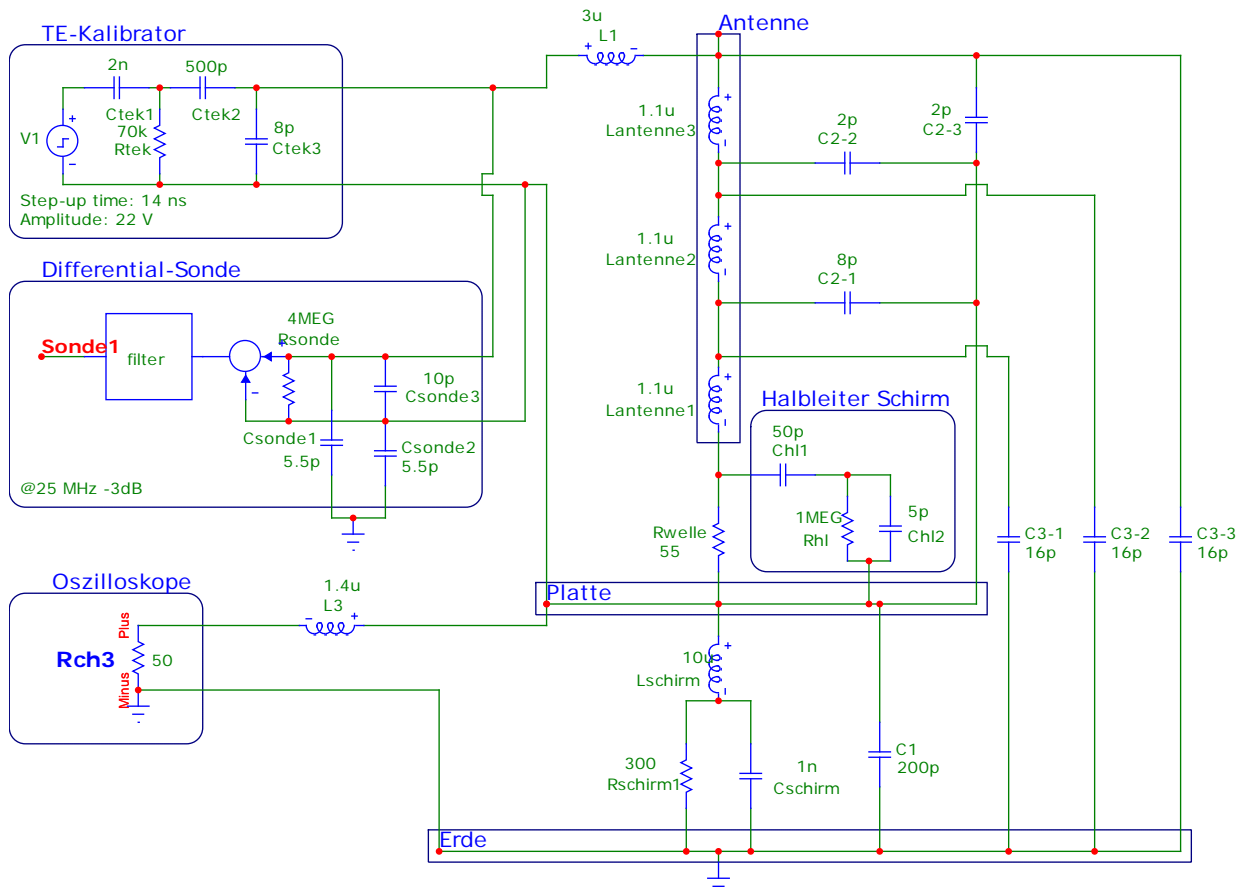


Figure 4-28: Circuit diagram of the on-site measurement - based on calculated values

Figure 4-29 shows the simulation results of the previous circuit on the right. The original measurement can be seen on the left side (same as Table 3-A). The two waveforms show some principal similarity. The time constants seem to be correct, the attenuation is the same and we can observe both the lower frequencies, both the higher frequencies with the right amplitude.

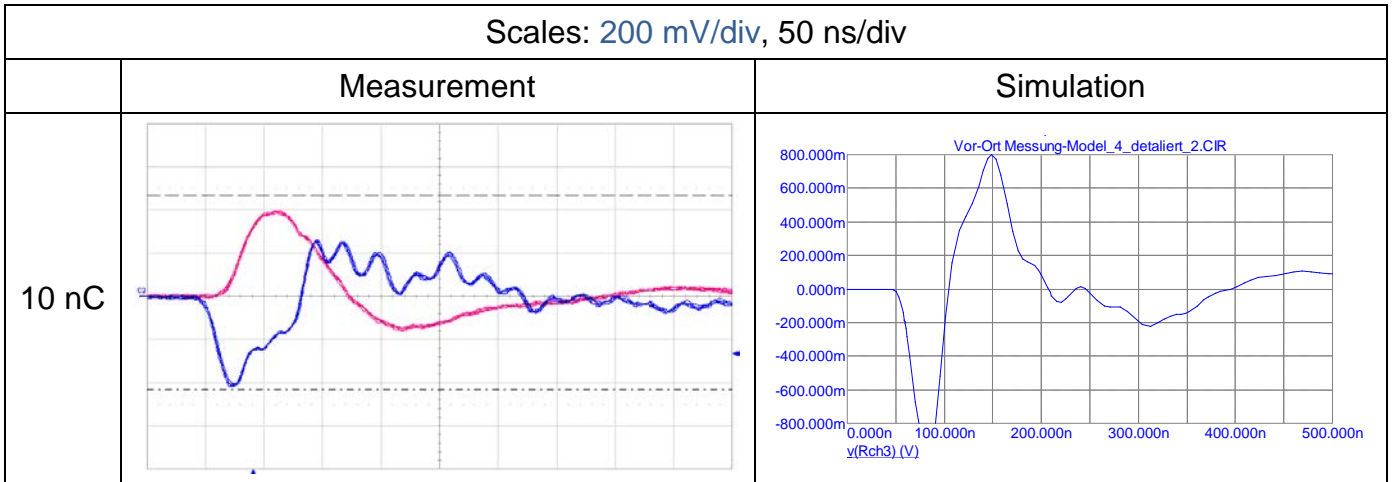


Figure 4-29: Comparison of measurement and simulation results - based on the calculated parameters

In this case the parameter variation was done manually and not with the optimization module, because it is lacking the function of binding different parameters together. Despite this, the waveform matched the measurement results after very quickly. Figure 4-30 shows the simulation circuit after the parameter variations.

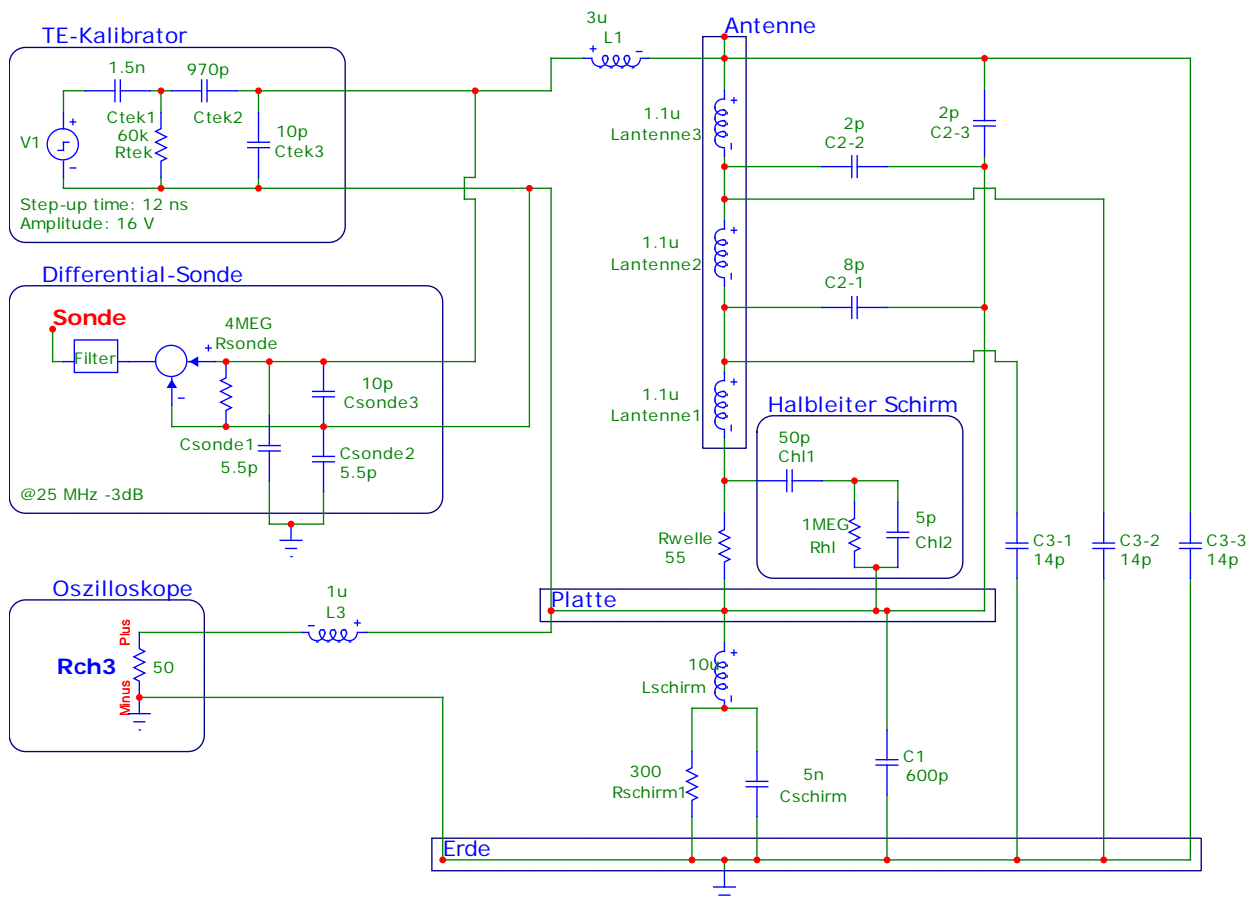


Figure 4-30: Circuit diagram of the on-site measurement - after parameter variation

Despite the complexity of the model, only a limited number of changes were necessary. The capacitances of the cable shielding were increased, the stray capacitances slightly decreased and the inductance of the measuring cable is also decreased.

To validate the measurement the model was investigated with different amounts of injected charge. The simulation was then compared with measured data from Table 3-A. Figure 4-31 shows the results: the measurement results from between the ground

and the shielding plate matches quite well. The differential probe signal also follows the measurement quite good, as long as the main harmonic does not fall into the 25 MHz range ($T=40$ ns), because in that domain the probe model has a smaller attenuation than in reality. The more intense higher frequency oscillation of the 10 nC case is due to the altered measurement setup in respect to the 50 nC case (see chapter 3.2.2.2 for details).

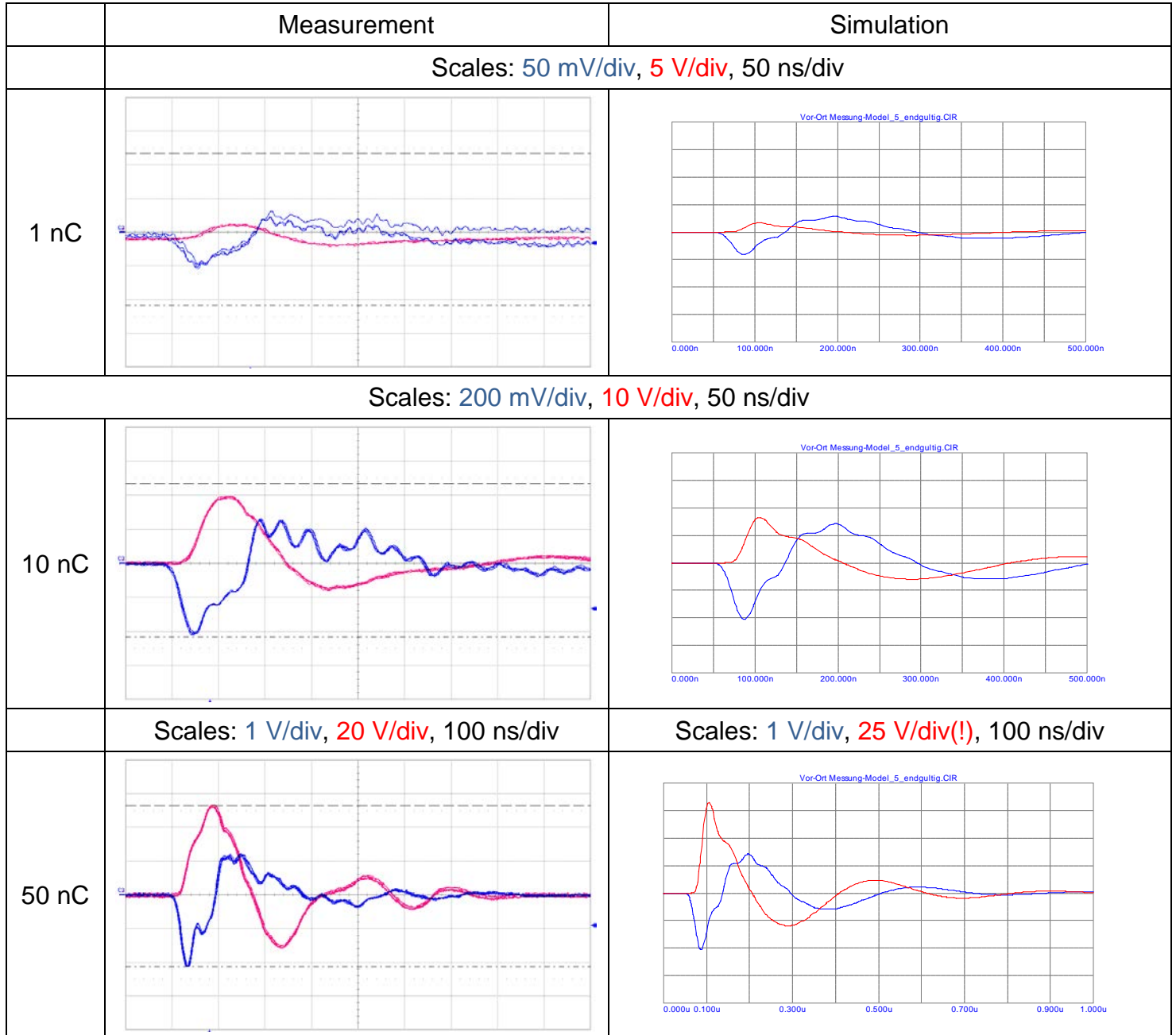


Figure 4-31: Comparison of measurement and simulation results - after parameter variation

4.4.7 Comparison with HV test installation

To investigate the validity of the measurement model, the simulation was extended to model the effect of the HV test setup. The test installation is consisted of a step-up transformer, HV coils and a capacitive divider as it was presented on Figure 3-4. Figure 4-32 shows the resulting circuit diagram. Due to the great distances between the measuring equipment huge loops formed, which have a calculated inductance of **10.5 μ H**. The capacitive divider was consisted of a **750 pF** and a 1500 nF capacitance, where the latter can be thus neglected. Unfortunately since the capacitive divider is also

relatively tall, it also has a significant inductance that is estimated to be $4 \mu\text{H}$. The greatest difficulty in this simulation is that the HV coil's high frequency behaviour is unknown. It is clear that it is capacitive, but finding a suitable circuit equivalent is difficult.

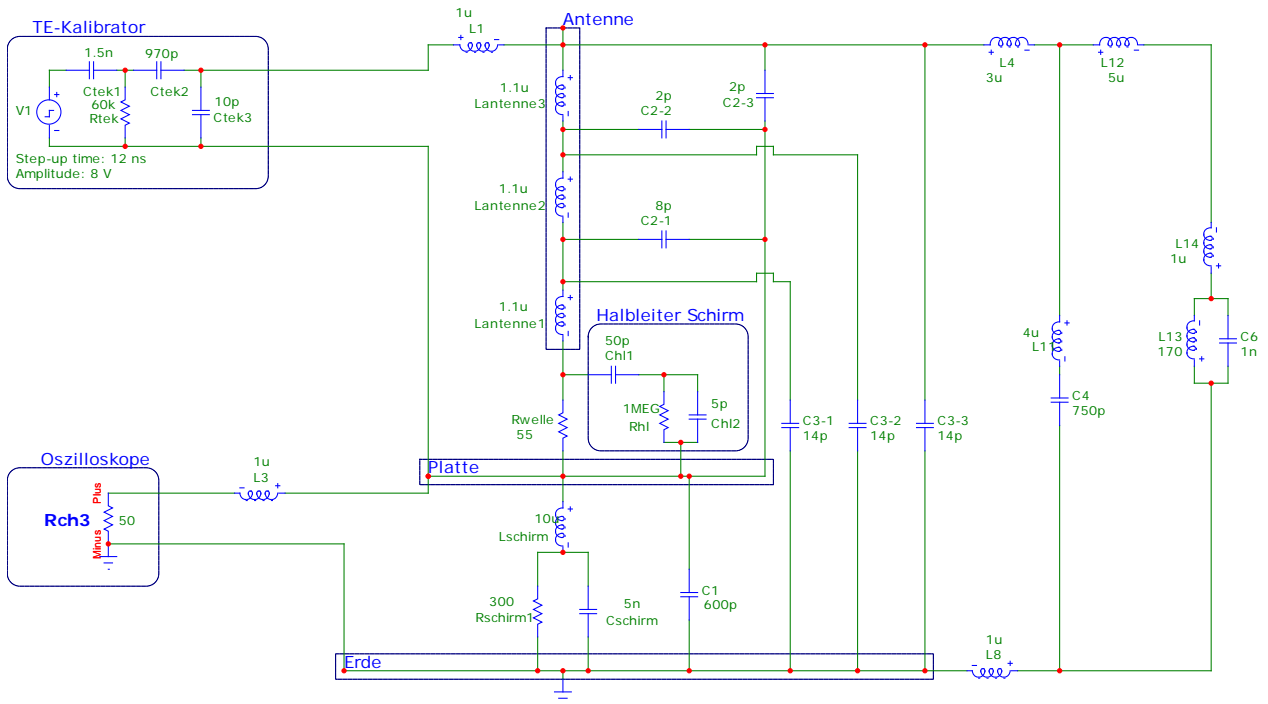


Figure 4-32: The on-site circuit extended with the HV test setup

Figure 4-33 shows the comparison between the simulation and the measurement. It is clear that the trend of the two waveforms is very similar, but there is a difference in amplitude by a factor five.

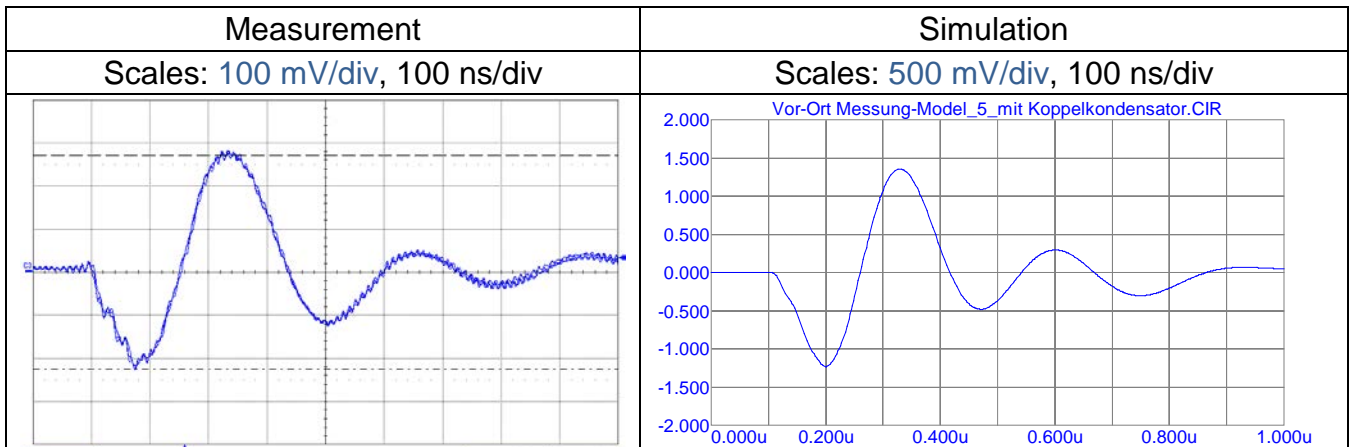


Figure 4-33: Comparison of measurement and simulation data on the on-site setup with HV installation

5. Analysis of created models

The aim of the following chapter is to draw practical conclusions based on the constructed models. From the beginning of the work special emphasis was put on such key questions as on which frequencies is it optimal to take measurements? Which are the key factors influencing the sensitivity of the measurement? And how does differences in the termination geometry influence the measurement sensitivity?

5.1 Analysis of frequency response

The frequency response of the on-site measurement model was investigated in the following way: I defined a transfer function where the input is a current source (modelling the Dirac-pulse of the partial discharge) and the output was the voltage measured over the oscilloscope. To find the dimensionless form of the response it must be also divided by one Ohm, as it is shown on Equation 5-1. This shows us on which frequencies can the partial discharge be best detected.

$$Y(f) = \frac{U_{R \text{ oscilloscope}}(f)}{I_{\text{calibrator}}(f)} \cdot \frac{1}{\Omega}$$

Equation 5-1: Dimensionless form of the partial discharge's transfer function

To investigate the difference between the calibration and an actual discharge the circuitry was made on Figure 5-1. In the case on the left the PD calibrator was simply replaced by the current input (marked with yellow). In the case on the right an actual partial discharge was simulated by connecting the current input directly between the cable core and the shielding.

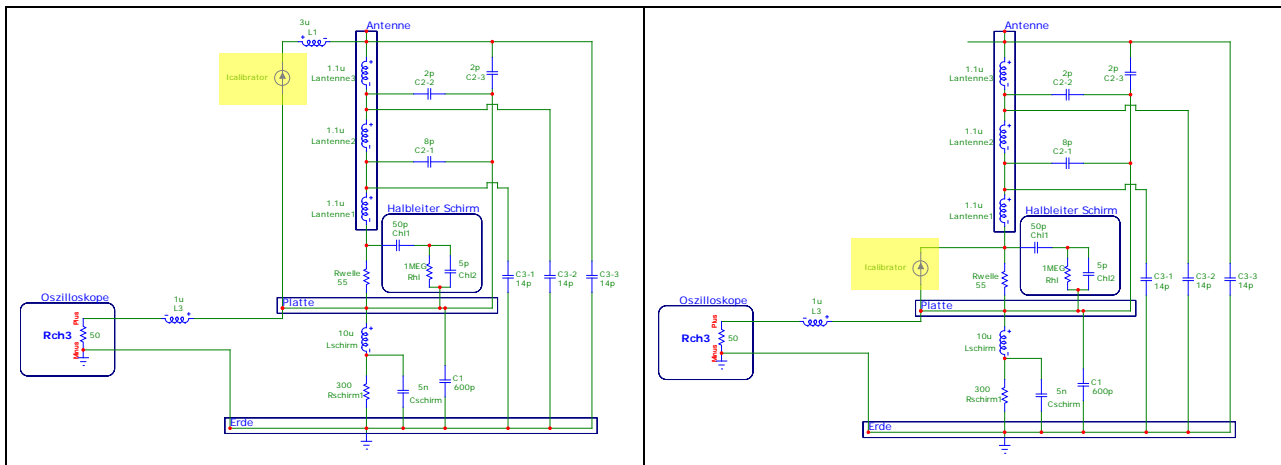


Figure 5-1: (left) Circuit of the calibration's transfer function
(right) Circuit of an actual partial discharge's transfer function

Figure 5-2 shows the resulting frequency responses. It is supporting the empirical experience that best sensitivity can be achieved in the 5-10 MHz domain using narrow band measuring system. The most peculiar feature of this comparison is attenuation difference in the 6-12 MHz domain. This is due to the fact that the inductances of the cable termination appear as high impedances. Therefore when the calibrating pulse must travel through the inductance of the cable loop, a much smaller voltage falls over the oscilloscope. This typically means a calibration error of 50% in the 6-12 MHz domain. It results, that following such calibration, the actual partial discharge may be more than twice of the detected discharge.

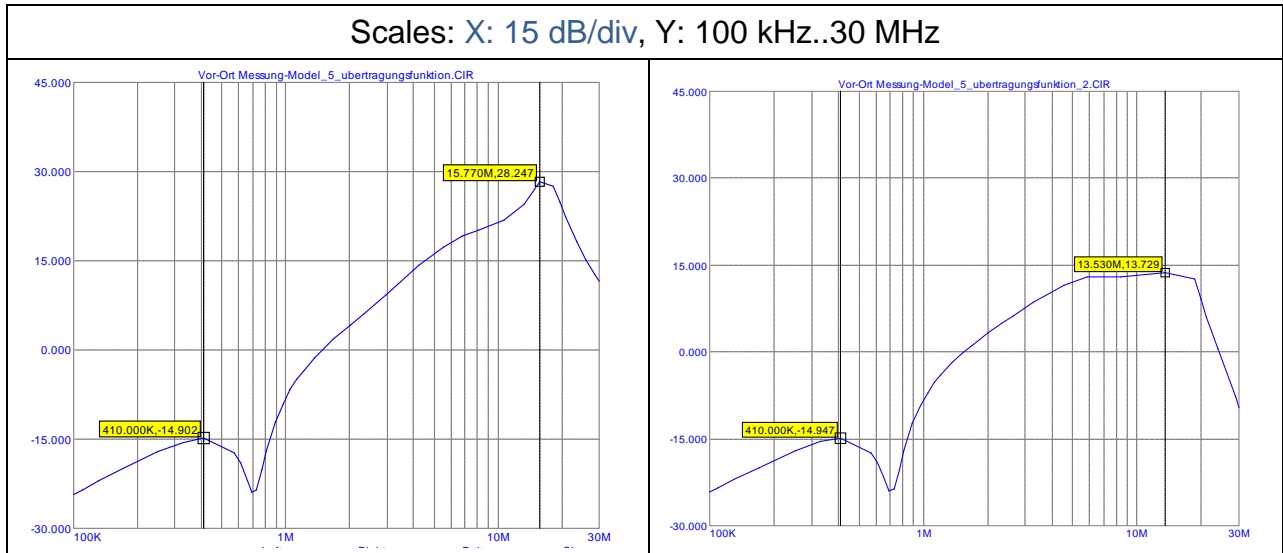


Figure 5-2: (left) Frequency response of a calibration pulse on a dB scale
 (right) Frequency response of an actual partial discharge on a dB scale

Figure 5-3 shows the difference in attenuation in the two different cases. The practical implication of this result may be that the calibration error in such high frequencies may be unacceptably high due to the large loop formed by the calibrator's cable and the core. This finding may have an effect on all calibrations and must be further investigated in detail. Therefore, in the following chapter, the calibration error is also going to be investigated.

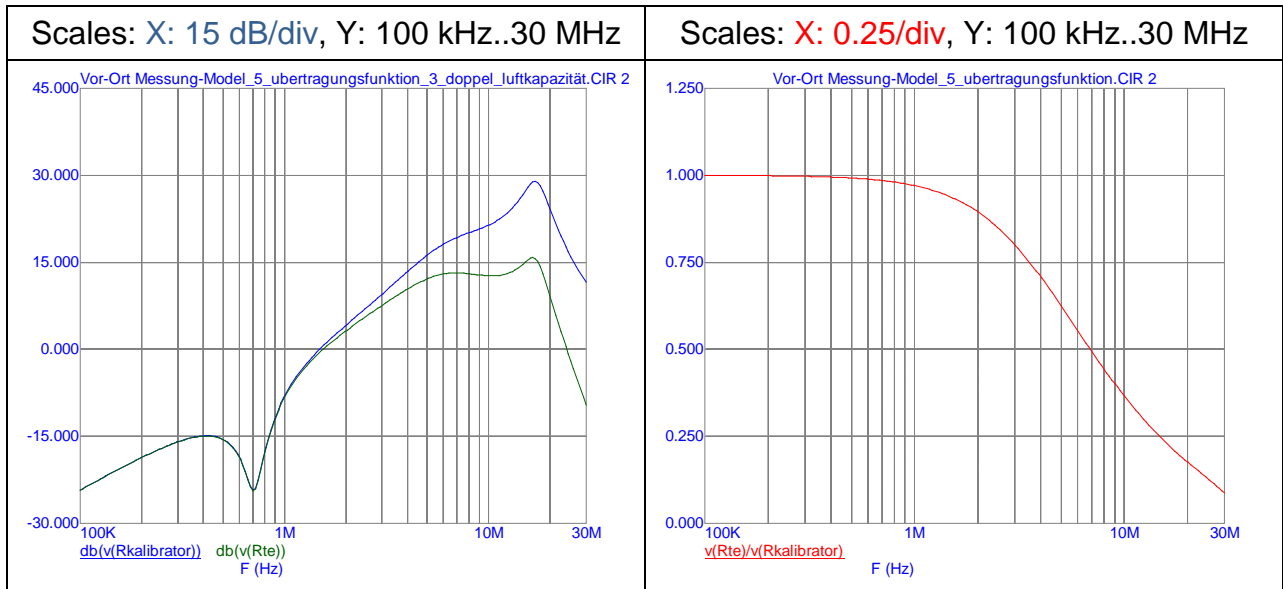


Figure 5-3: (left) Comparison of attenuations in the two different case
 (right) Ratio of the attenuation of the two different cases

5.2 Analysis of stray capacitance variations

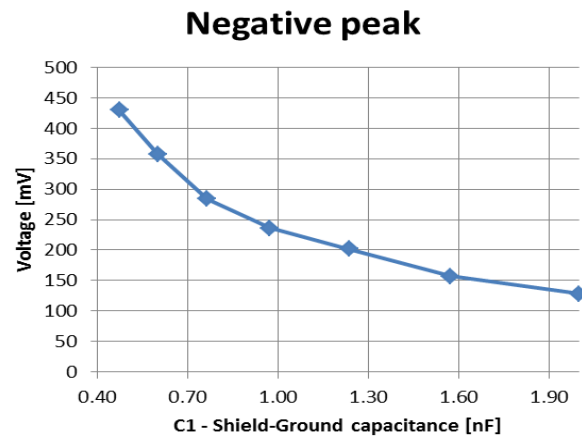
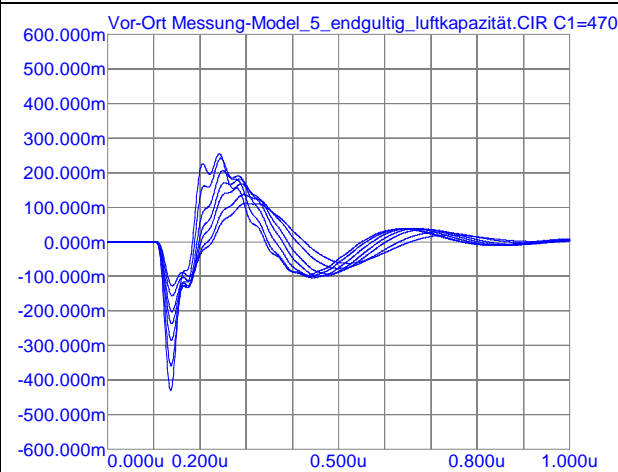
Firstly, it is going to be investigated what effect does the variation of stray capacitances have. The method of increasing or reducing stray capacitances is not part of this work, but also the previous intern conducted basic research in this field by adding metal toruses to the measurement setup. It must be noted that these findings apply only, when the construction of the cable termination is similar to the measured one.

5.2.1 $C_{\text{ground-shielding}}$

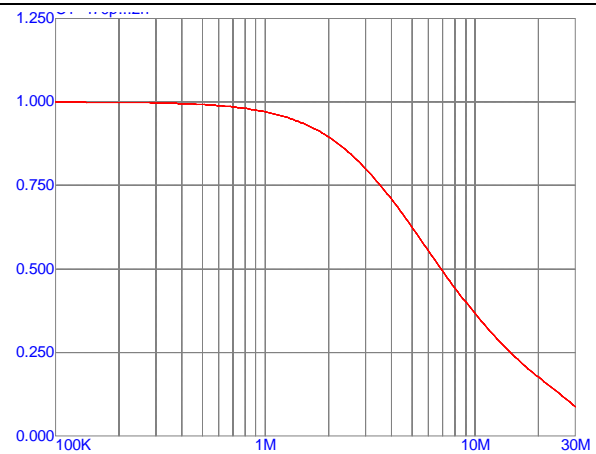
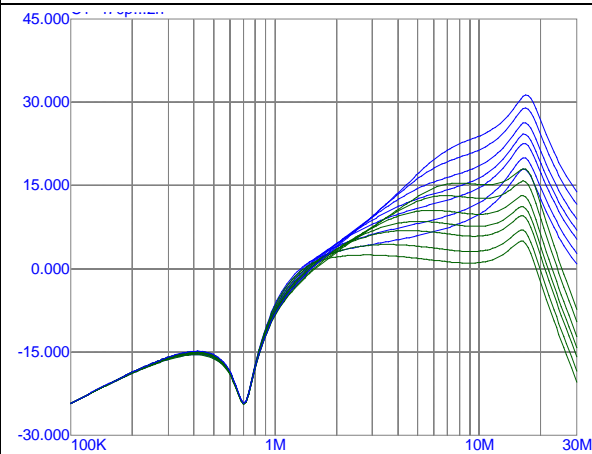
The first table always shows the values of parameter variation. The value marked with yellow is the original value, which was used during the creation of the model. The table below always shows the effect of the parameter variation.

$C_{\text{ground-shielding}}$ [nF]						
0.47	0.6	0.8	1.0	1.2	1.6	2.0

Measurement sensitivity



Calibration error



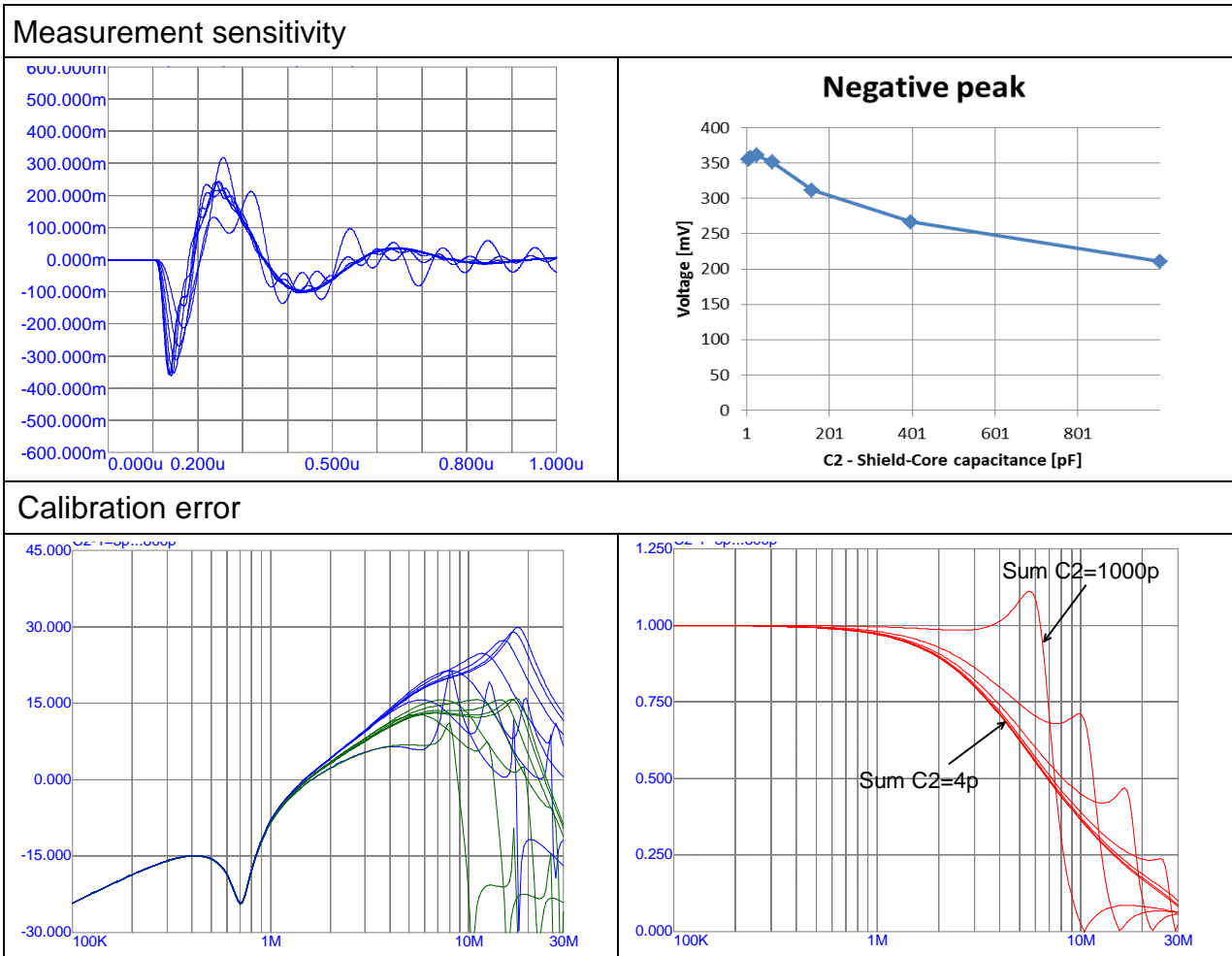
5-A. Table: The influence of the ground-shielding capacitance to the measurement sensitivity and to the Calibration error

Increasing the capacitance between the ground and shielding is decreasing the measurement sensitivity. Since this capacitance is mainly defined by the polarisation of the ground, there is little to be done about it, but it may be worth looking into possibilities of reducing this capacitance. The ground-shielding capacitance has no effect on the calibration error.

5.2.2 $C_{\text{Shielding-Core}}$

The shielding-core capacitance was consisting of three different capacitances (refer to Figure 4-30), therefore all three were altered proportionally.

Sum $C_{\text{Shielding-Core}}$ [pF]	4	10	25	63	158	398	1000
$C_{\text{Shielding-Core-1}}$ [pF]	3	8	20	50	127	318	800
$C_{\text{Shielding-Core-2}}$ [pF]	1	2	5	13	32	80	200
$C_{\text{Shielding-Core-3}}$ [pF]	1	2	5	13	32	80	200



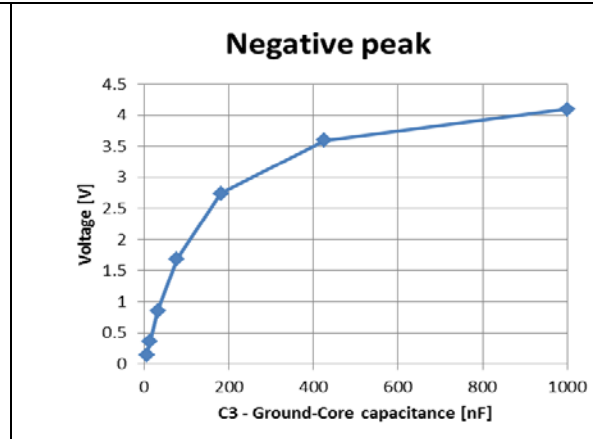
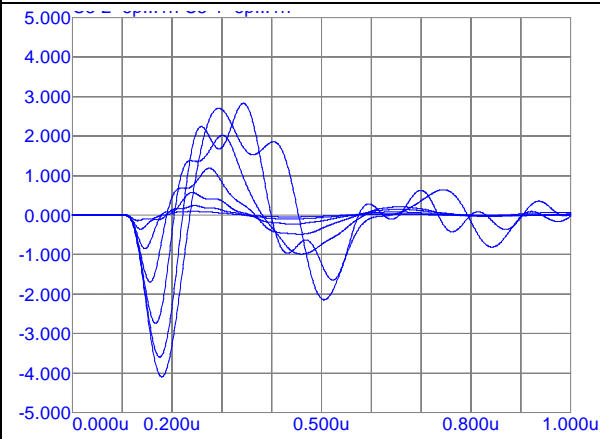
5-B. Table: The influence of the shielding-core capacitance to the measurement sensitivity and to the Calibration error

The shielding-core capacitance does not have a substantial effect on the measurement sensitivity. On the other hand it may mistune the resonance frequencies and thus may result in great differences in attenuation between the calibration and the measurement. It must be noted that in the simulation only the most significant resistances were considered, thus the amplification of the resonance frequencies may not be as definite as on the diagram.

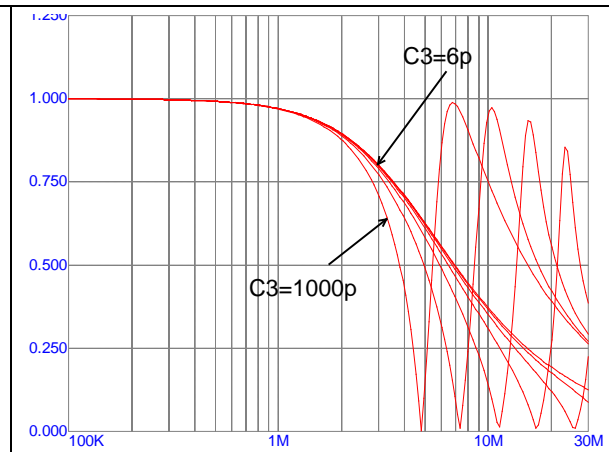
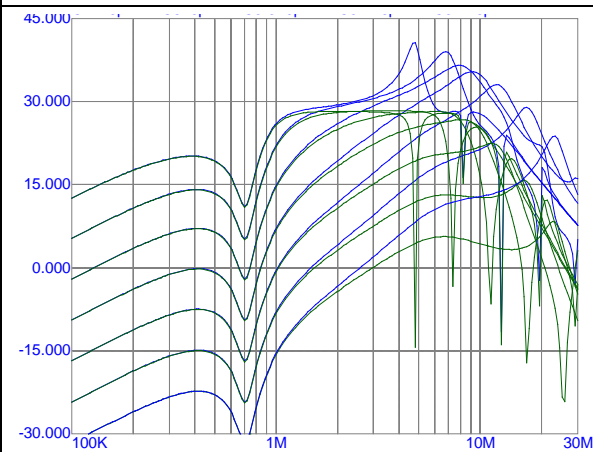
5.2.3 $C_{\text{Core-Ground}}$

$C_{\text{Core-Ground}}$ [pF]						
6	14	33	77	181	426	1000

Measurement sensitivity



Calibration error



5-C. Table: The influence of the core-ground capacitance to the measurement sensitivity and to the Calibration error

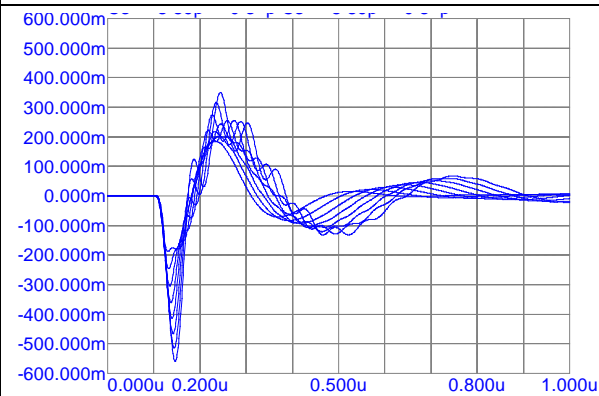
The core-ground capacitance has the greatest influence to the measurement sensitivity, since it is substituting the coupling capacitor. Increasing this stray capacitance is a priority for the better utilisation of the present measuring method. On the other hand increasing this capacitance may also generate resonances in the measurement domain.

5.3 Analysis of variations in the terminal's length

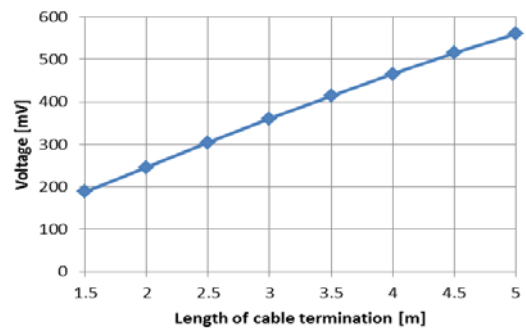
The terminal's length has a great influence on the measurement parameters, because it is altering not just the stray capacitances, but also the inductances of the measurement setup.

l [m]	Sum L [uH]	Lantenne [uH]	L1 [uH]	C3-1 [pF]	C3-2 [pF]	C3-3 [pF]
1.5	3.43	0.55	1.78	8.89	8.88	8.87
2	4.38	0.73	2.18	10.68	10.66	10.64
2.5	5.34	0.92	2.59	12.40	12.37	12.34
3	6.29	1.10	2.99	14.07	14.02	13.99
3.5	7.24	1.28	3.39	15.69	15.62	15.58
4	8.20	1.47	3.80	17.28	17.19	17.14
4.5	9.15	1.65	4.20	18.84	18.73	18.66
5	10.10	1.83	4.60	20.37	20.23	20.16

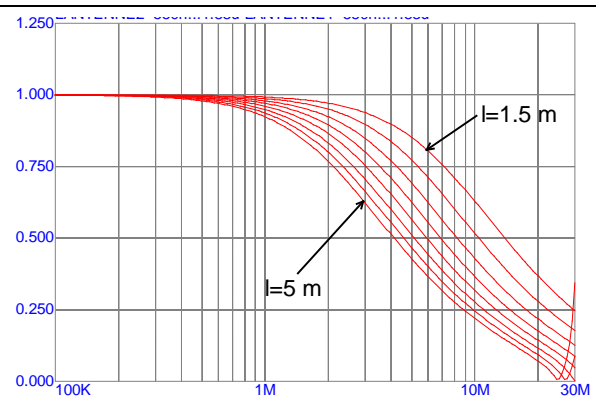
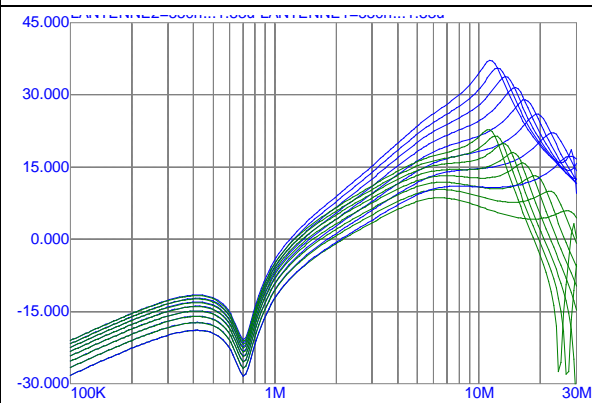
Measurement sensitivity



Negative peak



Calibration error



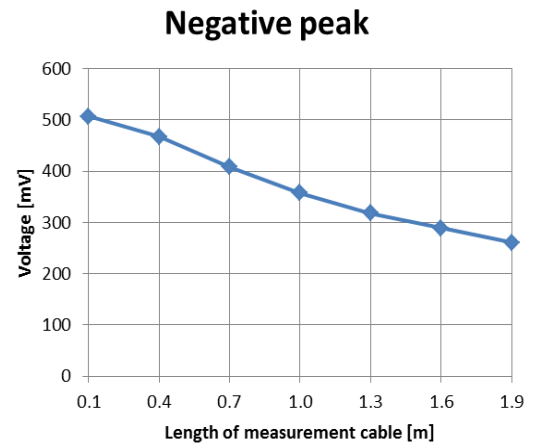
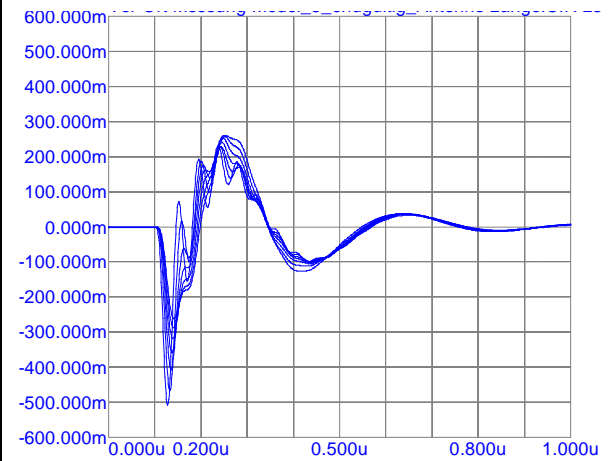
5-D. Table: The influence of the length of the terminal to the measurement sensitivity and to the Calibration error

The termination length is nearly linearly proportional with the measurement sensitivity. On the other hand, as expected a longer termination means a larger measurement cable loop and thus a greater difference between the calibrated values and the actual values.

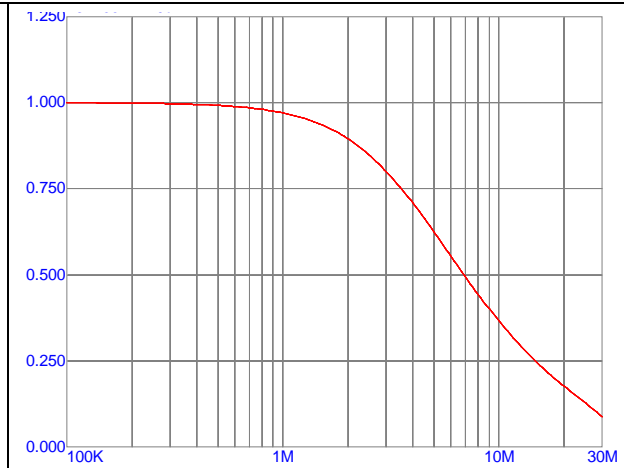
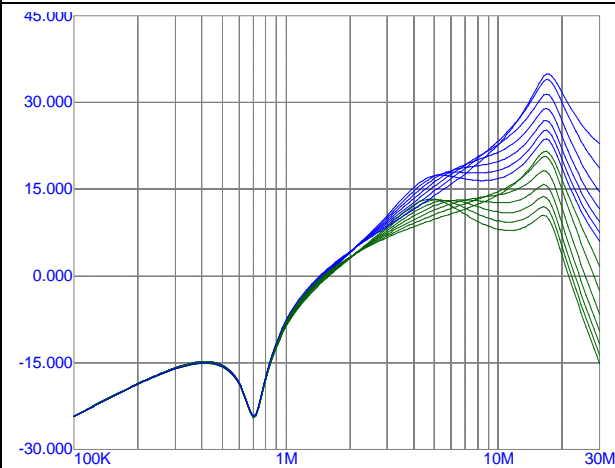
5.4 Analysis of the measurement cables' length

I [m]	0.1	0.4	0.7	1.0	1.3	1.6	1.9
L3 [uH]	0.1	0.4	0.7	1.0	1.3	1.6	1.9

Measurement sensitivity



Calibration error



5-E. Table: The influence of the measuring cable length to the measurement sensitivity and to the Calibration error

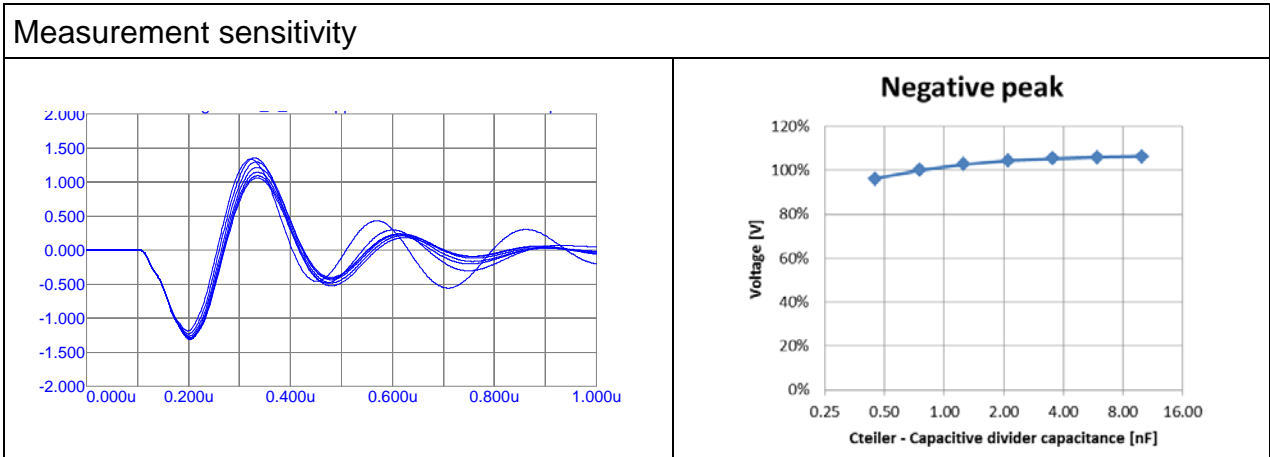
A longer measuring cable also means greater inductances in the system. Therefore it can be seen that the shorter the measuring cable is, the better the sensitivity. The measuring cable has no effect on the calibration error.

5.5 Analysis of the termination with capacitive divider

As detailed in chapter 4.4.7, the termination cannot be properly simulated with the HV installation, because the high frequency behaviour of the coils are not known. Despite this, the trend of the waveform was very similar and it may provide some qualitative information. Therefore the following diagrams are given in relative values.

5.5.1 Influence of the divider's capacitance

Cteiler [nF]						
0.45	0.75	1.26	2.11	3.55	5.96	10.00

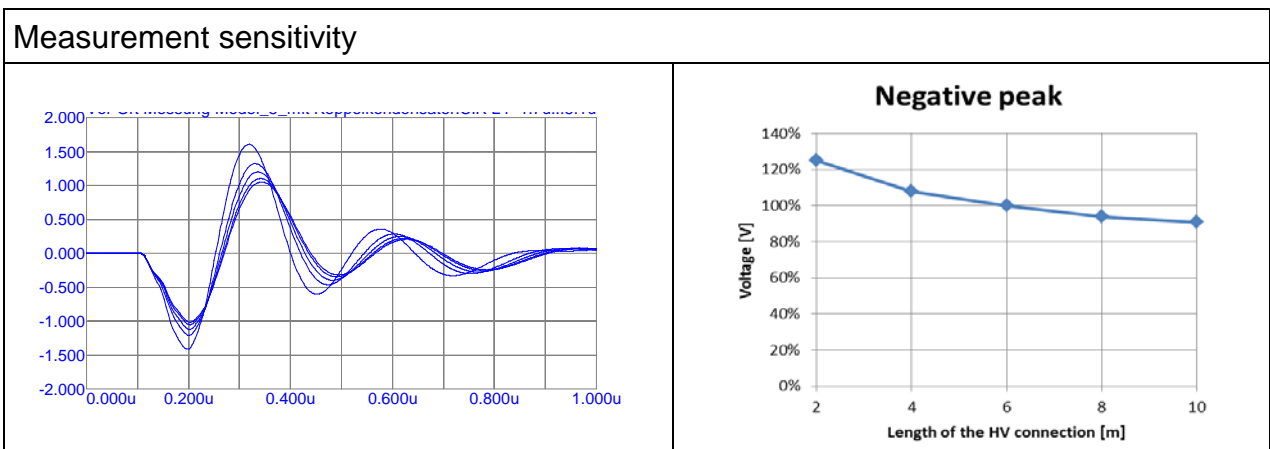


5-F. Table: The influence of the capacitance of the capacitive divider to the measurement sensitivity

The capacitive divider's capacitance is also expected to notably increase the sensitivity of the measurement, but the model suggests otherwise.

5.5.2 Influence of the HV connection's length

Iverbindung [m]	2	4	6	8	10
Lverbindung [uH]	1.7	3.2	4.0	4.7	5.1



5-G. Table: The influence of the HV connection's length to the measurement sensitivity

The HV connection is the metal pipe connecting the capacitive divider with the object under test (see Figure 3-4). It is accountable for a huge inductance in the measuring circuit and thus it is reducing the sensitivity.

6. Conclusion

An electric laboratory model of a cable termination was developed to investigate the possibility of partial discharge measurement without coupling capacitor. After the optimisation of the model, precise measurements were carried out and a computer simulation was performed using Micro-Cap. During an on-site test, measurements were conducted on a real cable termination as well. A digital model was built also for this case using the experiences from the previous model. The result is a more sophisticated model that proves to be reacting very well for the various inputs.

It was also assessed that an approximately 50% deviation can be observed between the calibrated values and the actual values of the apparent charge due to the different position of calibration equipment and real discharges that are captured in the typical measuring domain of 5-10 MHz. This finding calls for additional research in this area. This behaviour may not limit the applicability of the sensor in comparative analysis, but results great errors in a qualitative measurement, like the one conducted after the assembly of a cable termination.

A series of simulations was implemented to analyse the effects of changes in the PD measurement setup on the sensitivity and the calibration error.

Finally, my work opens the way for further developments, namely:

- Study of the calibration error by attaching a PD source to the BNC connector between the cable core and shielding table
- Detailed investigation of the high frequency behaviour of the cable shielding in the ground
- Investigation of the high frequency behaviour of the HV coils so the model can be extended with those elements
- Finding ways to increase/decrease the various stray capacitances in order to maximise the measurement sensitivity
- Reproduction of the on-site measurement on other cable terminations and comparison to the present results
- Reproduction of the measurements on the laboratory model using a larger and a smaller measuring cable loop to provide a better understanding of the influence of the loop inductance
- Implementation of a calibrator model with exponential voltage source for more precise results
- Implementation of inductance and capacitance calculations using field calculation software for more accurate results
- Development of a differential probe model with reproduction of the attenuation slump at 25 MHz

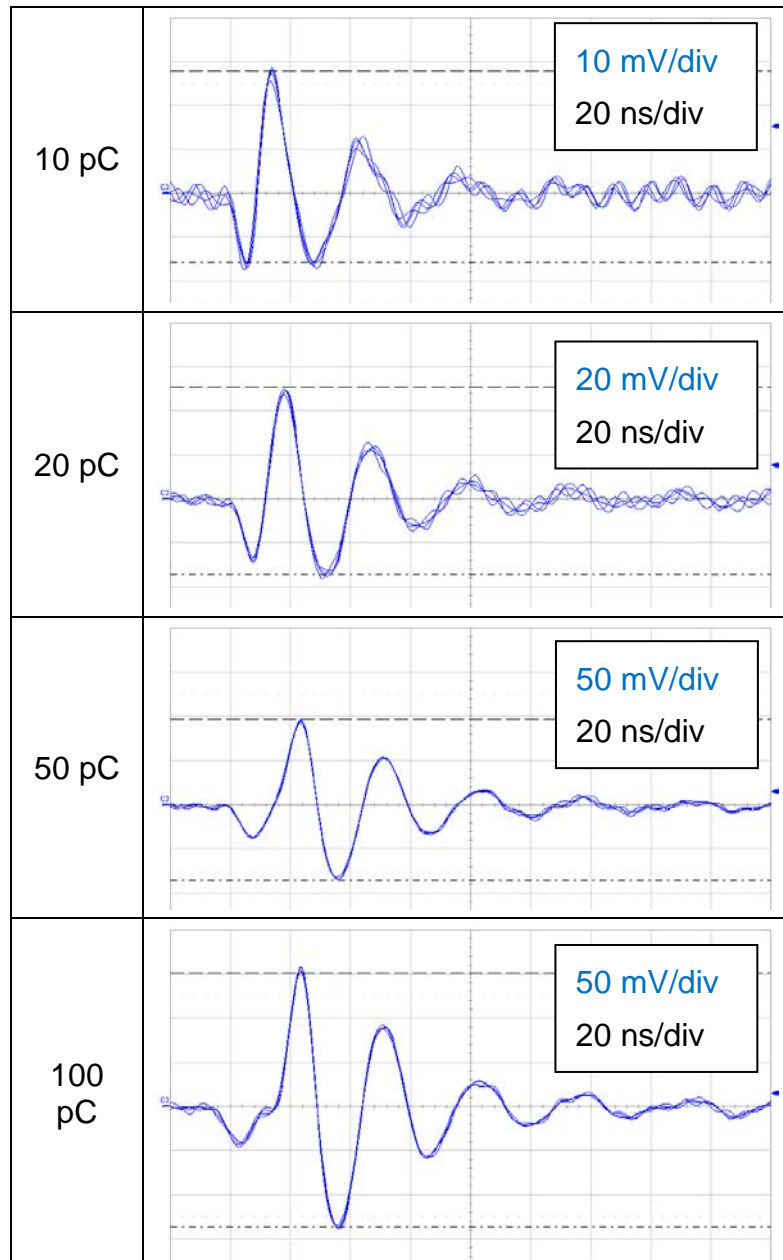
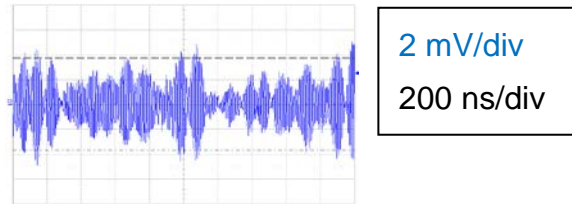
7. References

- [1] K. Uchida, H. Tanaka, K. Hirotsu: Study on detection for the defects of XLPE cable lines, 2. April 1996, <http://ieeexplore.ieee.org/stamp/stamp.jsp?tp=&arnumber=489320&tag=1>
- [2] C. Lee, L. Chih, M. Ciu, C. Huang, S. Yen, C. Haeng: Recognition of partial discharge defects in cable terminations, April 21-24, 2008, <http://ieeexplore.ieee.org/stamp/stamp.jsp?tp=&arnumber=4580513>
- [3] IEC International Standard 60270 Third Edition 2000-12
- [4] W. S. Zaengl: High Voltage Engineering Fundamentals, second edition, Oxford, 2005
- [5] H.J. Weber (Tettex Instruments AG): Partial discharge measuring techniques information manual, 1990
- [6] O. Bergius: FKH internship report, Zürich, 2012.
- [7] HIGHVOLT Prüftechnik Dresden GmbH, 2012. [Online]. Available: <http://www.transform.net/portaldata/1/Resources/HV/Downloads/6-33-3.pdf>. [Accessed 20 09 2013].
- [8] C. Hanser: Taschenbuch Elektrotechnik - Band 1, Page 95, 1. Volume, 1976.
- [9] Meinke und Gundlach: Taschenbuch der Hochfrequenztechnik - Band 1: Grundlagen, Seite B13-B14, 1992.
- [10] Eddy Current Technology Incorporated, "Skin depth frequency table," 12 April 2013. [Online]. Available: <http://eddy-current.com/skin-depth-frequency-table-2/>. [Accessed 20 September 2013].
- [11] C. Hanser: Taschenbuch Elektrotechnik - Band 1, Page 56, 1. Volume, 1976.

Appendices

I. Appendix: Results of the laboratory model measurements

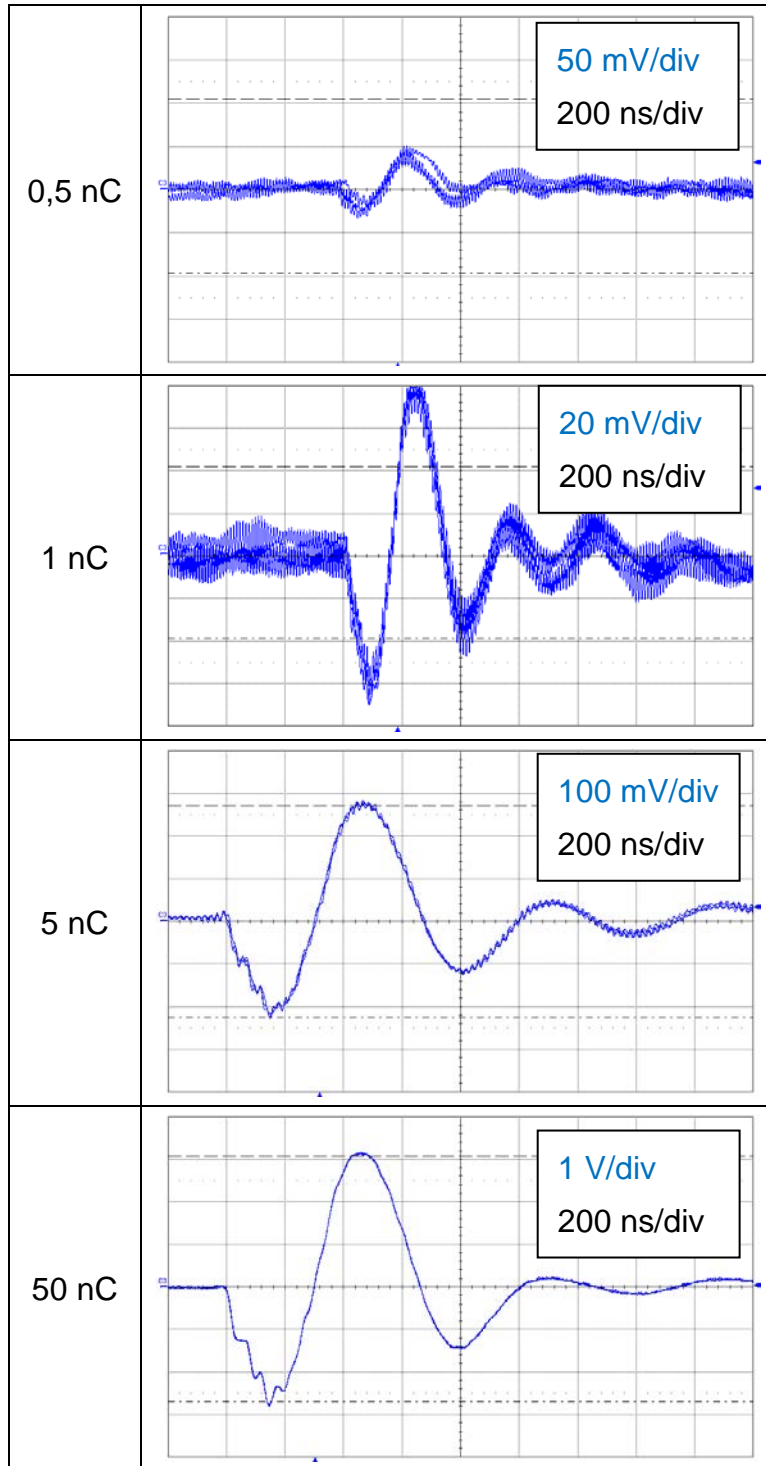
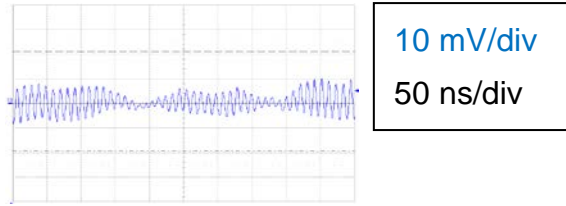
Background noise:



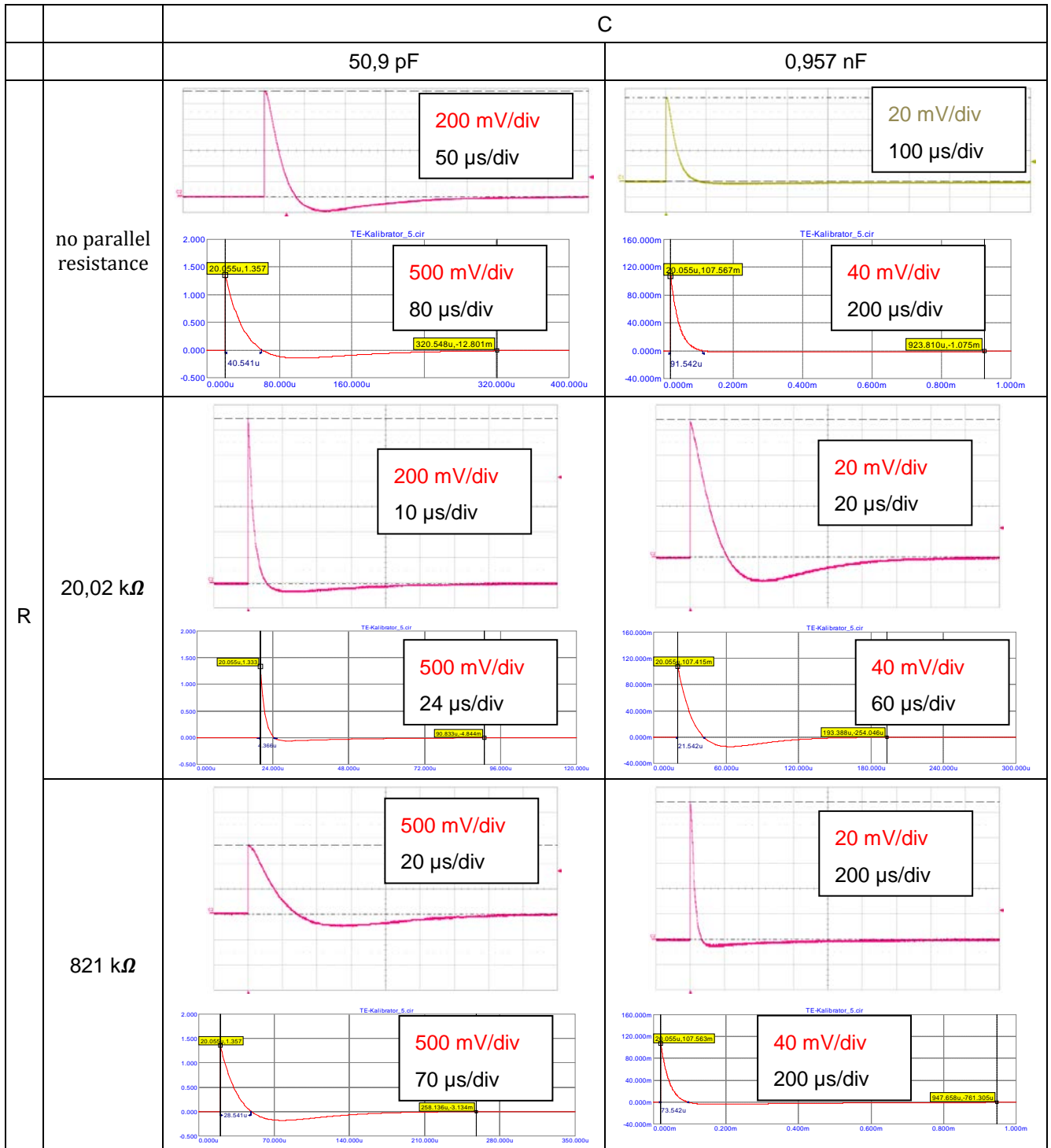
It can be observed, that the first negative swing is acting nonlinearly. Especially interesting is the inflection point at the 100 pC. It might be due to the fact, that the voltage step of the calibrator cannot follow such a steep function. Supposedly this effect could be modelled if the voltage source of the calibrator was set to be an exponential function, rather than a ramp.

II. Appendix: Results of the on-site measurement with HV test installation

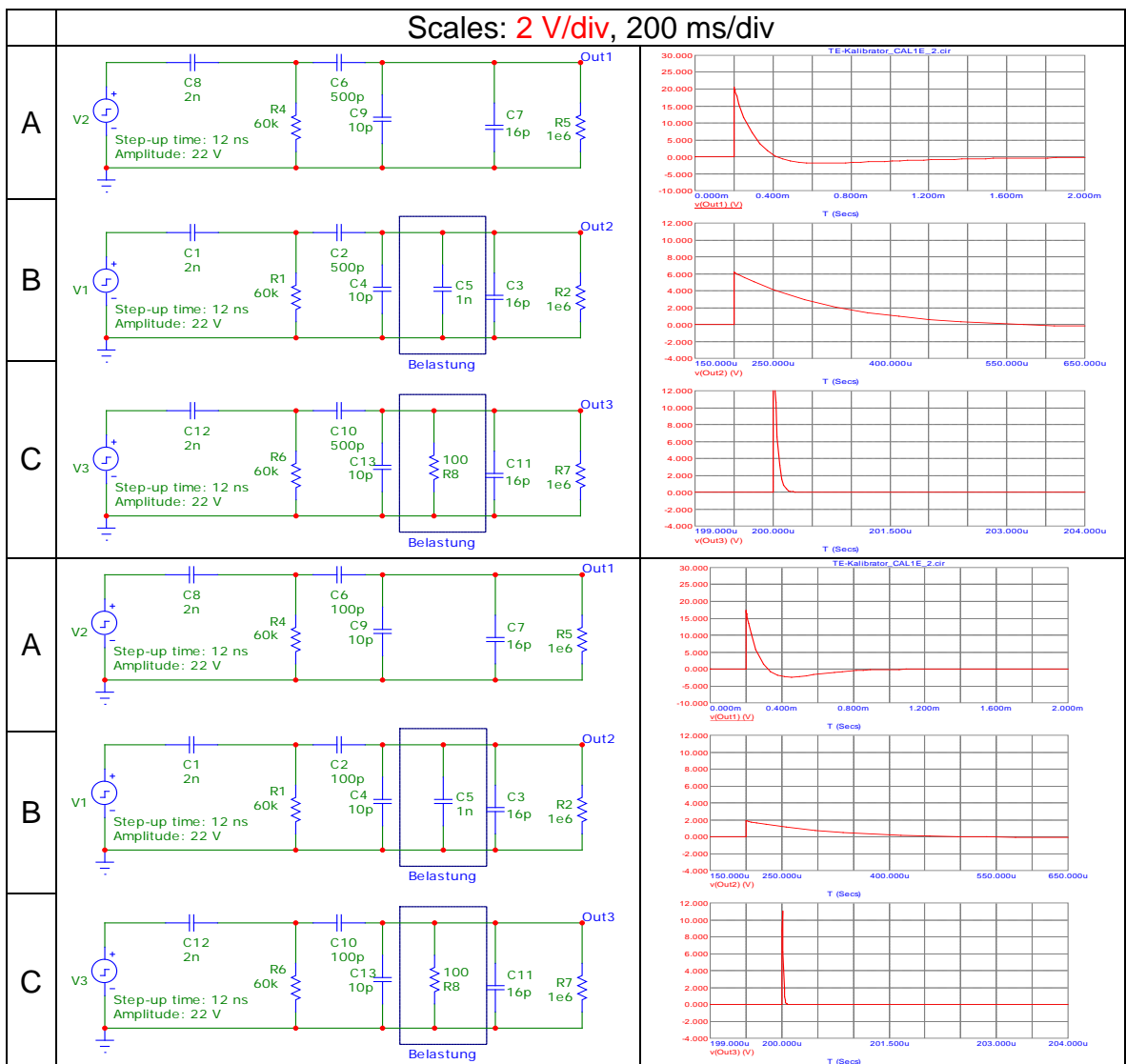
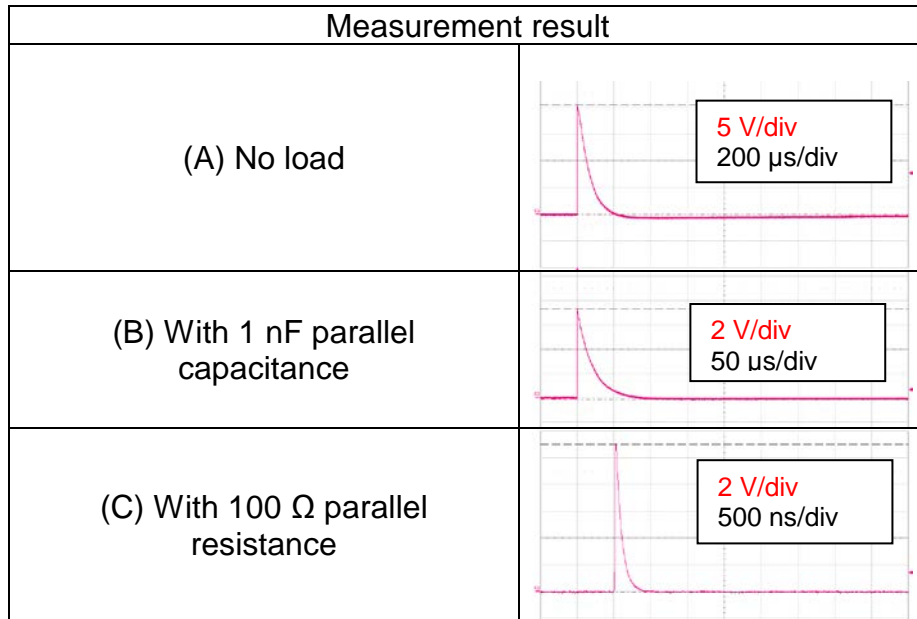
Background noise:



III. Appendix: CAL1A measurement results and comparison of simulation with different loads



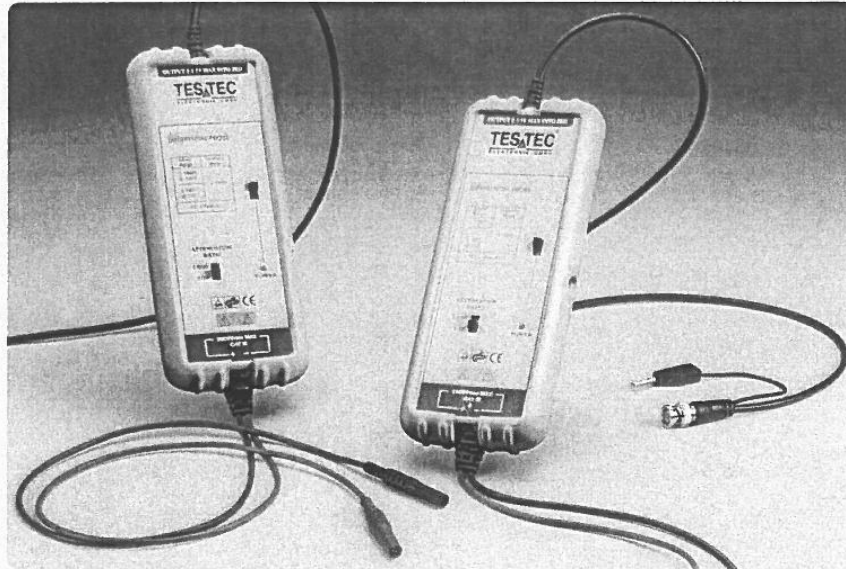
IV. Appendix: CAL1E measurement results and comparison of simulation with different loads



(For comparable results the same scaling was used in the three tables.)

V. Appendix: Datasheet of the TT-SI 9001 Differential probe

**Aktive Differential-Tastköpfe / Active Differential Probes
TT-SI 9001, TT-SI 9002**



Specifications	Type	TT-SI 9001	TT-SI 9002
Ordernumber		15101	15102
Bandwidth		DC to 25MHz (-3dB)	DC to 25MHz (-3dB)
Attenuation Ratio		1:10 / 1:100	1:20 / 1:200
Accuracy		±2%	±2%
Rise Time		14ns	14ns
Input Impedance		4MΩ // 5,5pF each side to ground	4MΩ // 5,5pF each side to ground
Input Voltage			
- Differential Range	1:10	±70V (DC + peak AC) or 70Vrms	1:20 ±140V (DC + peak AC) or 140Vrms
	1:100	±700V (DC + peak AC) or 700Vrms	1:200 ±1400V (DC + peak AC) or 1000Vrms
- Common Mode Range	1:10	±700V (DC + peak AC) or 700Vrms	1:20 ±1400V (DC + peak AC) or 1000Vrms
	1:100	±700V (DC + peak AC) or 700Vrms	1:200 ±1400V (DC + peak AC) or 1000Vrms
- Absolute max. Voltage CAT III	1:10	±1400V (DC + peak AC) or 1000Vrms	1:20 ±1400V (DC + peak AC) or 1000Vrms
	1:100	±1400V (DC + peak AC) or 1000Vrms	1:200 ±1400V (DC + peak AC) or 1000Vrms
Output			
- Swing		±7V (into 2kΩ load)	±7V (into 2kΩ load)
- Offset (typical)		<±5mV	<±5mV
- Noise (typical)		0,7mVrms	0,7mVrms
- Source Impedance (typical)		1Ω @ 1kHz, 8Ω @ 1MHz	1Ω @ 1kHz, 8Ω @ 1MHz
CMRR (typical)		-86dB @ 50Hz, -66dB @ 20kHz	-80dB @ 50Hz, -60dB @ 20kHz

Technische Änderungen vorbehalten / All specifications and characteristics are subject to change without notice

Power requirements: 4 x AA Cells or Mains Adaptor 6VDC/60mA or regulated 9VDC/40mA

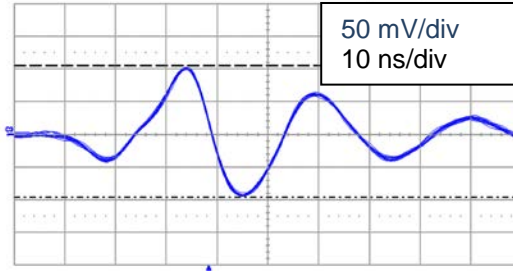
Dimensions: (L x W x H) 170mm x 63mm x 21mm

Length: BNC Cable 95cm - Input Leads 45cm

Weight: 400g (Probe and PVC-Jacket)

VI. Appendix: Parameter fine-tuning to the Laboratory model

Measurement result:



RMS deviation	Parameter setting	Simulation result																																																																																																														
8.13	<table border="1"> <thead> <tr> <th>Find</th> <th>Parameter</th> <th>Low</th> <th>High</th> <th>Step</th> <th>Current</th> <th>Optimized</th> </tr> </thead> <tbody> <tr><td>- + Get</td><td>PUL PULSE(P1)</td><td>6n</td><td>15n</td><td>5n</td><td>14.87In</td><td>14.87In</td></tr> <tr><td>- + Get</td><td>PUL PULSE(P2)</td><td>23n</td><td>29n</td><td></td><td>24.98n</td><td>24.98n</td></tr> <tr><td>- + Get</td><td>C1</td><td>15p</td><td>45p</td><td>3p</td><td>16.557p</td><td>16.557p</td></tr> <tr><td>- + Get</td><td>C2</td><td>30p</td><td>90p</td><td>10p</td><td>30p</td><td>30p</td></tr> <tr><td>- + Get</td><td>C3</td><td>6p</td><td>14p</td><td>4p</td><td>11.952p</td><td>11.952p</td></tr> <tr><td>- + Get</td><td>L1</td><td>0.6u</td><td>1.8u</td><td>4u</td><td>1.8u</td><td>1.8u</td></tr> <tr><td>- + Get</td><td>LANTENNE</td><td>0.1u</td><td>0.9u</td><td>0.5u</td><td>207.586n</td><td>207.586n</td></tr> </tbody> </table> <table border="1"> <thead> <tr> <th>-That</th> <th>Performance Function Expression</th> <th>To</th> <th>Current</th> <th>Optimized</th> <th>Error</th> </tr> </thead> <tbody> <tr><td>Equates</td><td>Valley_X(v(Rch3),1,1)*10^-9</td><td>18</td><td>23.039</td><td>23.039</td><td>5.039</td></tr> <tr><td>Equates</td><td>Valley_Y(v(Rch3),1,1)*10^-3</td><td>-40</td><td>-48.596</td><td>-48.596</td><td>-8.596</td></tr> <tr><td>Equates</td><td>High_X(v(Rch3),1)*10^-9</td><td>34</td><td>33.98</td><td>33.98</td><td>-20m</td></tr> <tr><td>Equates</td><td>High_Y(v(Rch3),1)*10^-3</td><td>100</td><td>99.995</td><td>99.995</td><td>-4.645m</td></tr> <tr><td>Equates</td><td>Low_X(v(Rch3),1)*10^-9</td><td>45</td><td>45.98</td><td>45.98</td><td>980m</td></tr> <tr><td>Equates</td><td>Low_Y(v(Rch3),1)*10^-3</td><td>-95</td><td>-88.695</td><td>-88.695</td><td>6.305</td></tr> <tr><td>Equates</td><td>Y_Range(v(Rch3),1,1,70n,100n)*10^-3</td><td>70</td><td>65.183</td><td>65.183</td><td>-4.817</td></tr> <tr><td>Equates</td><td>Period(v(Rch3),1,2)*10^-10</td><td>290</td><td>260.62</td><td>260.62</td><td>-29.38</td></tr> </tbody> </table>	Find	Parameter	Low	High	Step	Current	Optimized	- + Get	PUL PULSE(P1)	6n	15n	5n	14.87In	14.87In	- + Get	PUL PULSE(P2)	23n	29n		24.98n	24.98n	- + Get	C1	15p	45p	3p	16.557p	16.557p	- + Get	C2	30p	90p	10p	30p	30p	- + Get	C3	6p	14p	4p	11.952p	11.952p	- + Get	L1	0.6u	1.8u	4u	1.8u	1.8u	- + Get	LANTENNE	0.1u	0.9u	0.5u	207.586n	207.586n	-That	Performance Function Expression	To	Current	Optimized	Error	Equates	Valley_X(v(Rch3),1,1)*10^-9	18	23.039	23.039	5.039	Equates	Valley_Y(v(Rch3),1,1)*10^-3	-40	-48.596	-48.596	-8.596	Equates	High_X(v(Rch3),1)*10^-9	34	33.98	33.98	-20m	Equates	High_Y(v(Rch3),1)*10^-3	100	99.995	99.995	-4.645m	Equates	Low_X(v(Rch3),1)*10^-9	45	45.98	45.98	980m	Equates	Low_Y(v(Rch3),1)*10^-3	-95	-88.695	-88.695	6.305	Equates	Y_Range(v(Rch3),1,1,70n,100n)*10^-3	70	65.183	65.183	-4.817	Equates	Period(v(Rch3),1,2)*10^-10	290	260.62	260.62	-29.38	<p>Scales: 50 mV/div, 10 ns/div</p>
Find	Parameter	Low	High	Step	Current	Optimized																																																																																																										
- + Get	PUL PULSE(P1)	6n	15n	5n	14.87In	14.87In																																																																																																										
- + Get	PUL PULSE(P2)	23n	29n		24.98n	24.98n																																																																																																										
- + Get	C1	15p	45p	3p	16.557p	16.557p																																																																																																										
- + Get	C2	30p	90p	10p	30p	30p																																																																																																										
- + Get	C3	6p	14p	4p	11.952p	11.952p																																																																																																										
- + Get	L1	0.6u	1.8u	4u	1.8u	1.8u																																																																																																										
- + Get	LANTENNE	0.1u	0.9u	0.5u	207.586n	207.586n																																																																																																										
-That	Performance Function Expression	To	Current	Optimized	Error																																																																																																											
Equates	Valley_X(v(Rch3),1,1)*10^-9	18	23.039	23.039	5.039																																																																																																											
Equates	Valley_Y(v(Rch3),1,1)*10^-3	-40	-48.596	-48.596	-8.596																																																																																																											
Equates	High_X(v(Rch3),1)*10^-9	34	33.98	33.98	-20m																																																																																																											
Equates	High_Y(v(Rch3),1)*10^-3	100	99.995	99.995	-4.645m																																																																																																											
Equates	Low_X(v(Rch3),1)*10^-9	45	45.98	45.98	980m																																																																																																											
Equates	Low_Y(v(Rch3),1)*10^-3	-95	-88.695	-88.695	6.305																																																																																																											
Equates	Y_Range(v(Rch3),1,1,70n,100n)*10^-3	70	65.183	65.183	-4.817																																																																																																											
Equates	Period(v(Rch3),1,2)*10^-10	290	260.62	260.62	-29.38																																																																																																											
7.11	<table border="1"> <thead> <tr> <th>Find</th> <th>Parameter</th> <th>Low</th> <th>High</th> <th>Step</th> <th>Current</th> <th>Optimized</th> </tr> </thead> <tbody> <tr><td>- + Get</td><td>PUL PULSE(P1)</td><td>7n</td><td>11n</td><td>5n</td><td>10.966n</td><td>10.966n</td></tr> <tr><td>- + Get</td><td>PUL PULSE(P2)</td><td>25n</td><td>29n</td><td></td><td>25n</td><td>25n</td></tr> <tr><td>- + Get</td><td>C1</td><td>20p</td><td>40p</td><td>8p</td><td>20p</td><td>20p</td></tr> <tr><td>- + Get</td><td>C2</td><td>30p</td><td>90p</td><td>10p</td><td>30p</td><td>30p</td></tr> <tr><td>- + Get</td><td>C3</td><td>6p</td><td>14p</td><td>4p</td><td>14p</td><td>14p</td></tr> <tr><td>- + Get</td><td>L1</td><td>1.6u</td><td>2.1u</td><td>4u</td><td>2.1u</td><td>2.1u</td></tr> <tr><td>- + Get</td><td>LANTENNE</td><td>0.1u</td><td>0.3u</td><td>0.5u</td><td>291.961n</td><td>291.961n</td></tr> </tbody> </table> <table border="1"> <thead> <tr> <th>-That</th> <th>Performance Function Expression</th> <th>To</th> <th>Current</th> <th>Optimized</th> <th>Error</th> </tr> </thead> <tbody> <tr><td>Equates</td><td>Valley_X(v(Rch3),1,0)*10^-9</td><td>18</td><td>20.355</td><td>20.355</td><td>2.355</td></tr> <tr><td>Equates</td><td>Valley_Y(v(Rch3),1,1)*10^-3</td><td>-40</td><td>-42.884</td><td>-42.884</td><td>-2.884</td></tr> <tr><td>Equates</td><td>High_X(v(Rch3),1)*10^-9</td><td>34</td><td>34.293</td><td>34.293</td><td>293.236m</td></tr> <tr><td>Equates</td><td>High_Y(v(Rch3),1)*10^-3</td><td>100</td><td>92.159</td><td>92.159</td><td>-7.841</td></tr> <tr><td>Equates</td><td>Low_X(v(Rch3),1)*10^-9</td><td>45</td><td>46.293</td><td>46.293</td><td>1.293</td></tr> <tr><td>Equates</td><td>Low_Y(v(Rch3),1)*10^-3</td><td>-95</td><td>-88.415</td><td>-88.415</td><td>6.585</td></tr> <tr><td>Equates</td><td>Y_Range(v(Rch3),1,1,70n,100n)*10^-3</td><td>70</td><td>56.224</td><td>56.224</td><td>-13.776</td></tr> <tr><td>Equates</td><td>Period(v(Rch3),1,2)*10^-10</td><td>290</td><td>277.08</td><td>277.08</td><td>-12.92</td></tr> </tbody> </table>	Find	Parameter	Low	High	Step	Current	Optimized	- + Get	PUL PULSE(P1)	7n	11n	5n	10.966n	10.966n	- + Get	PUL PULSE(P2)	25n	29n		25n	25n	- + Get	C1	20p	40p	8p	20p	20p	- + Get	C2	30p	90p	10p	30p	30p	- + Get	C3	6p	14p	4p	14p	14p	- + Get	L1	1.6u	2.1u	4u	2.1u	2.1u	- + Get	LANTENNE	0.1u	0.3u	0.5u	291.961n	291.961n	-That	Performance Function Expression	To	Current	Optimized	Error	Equates	Valley_X(v(Rch3),1,0)*10^-9	18	20.355	20.355	2.355	Equates	Valley_Y(v(Rch3),1,1)*10^-3	-40	-42.884	-42.884	-2.884	Equates	High_X(v(Rch3),1)*10^-9	34	34.293	34.293	293.236m	Equates	High_Y(v(Rch3),1)*10^-3	100	92.159	92.159	-7.841	Equates	Low_X(v(Rch3),1)*10^-9	45	46.293	46.293	1.293	Equates	Low_Y(v(Rch3),1)*10^-3	-95	-88.415	-88.415	6.585	Equates	Y_Range(v(Rch3),1,1,70n,100n)*10^-3	70	56.224	56.224	-13.776	Equates	Period(v(Rch3),1,2)*10^-10	290	277.08	277.08	-12.92	
Find	Parameter	Low	High	Step	Current	Optimized																																																																																																										
- + Get	PUL PULSE(P1)	7n	11n	5n	10.966n	10.966n																																																																																																										
- + Get	PUL PULSE(P2)	25n	29n		25n	25n																																																																																																										
- + Get	C1	20p	40p	8p	20p	20p																																																																																																										
- + Get	C2	30p	90p	10p	30p	30p																																																																																																										
- + Get	C3	6p	14p	4p	14p	14p																																																																																																										
- + Get	L1	1.6u	2.1u	4u	2.1u	2.1u																																																																																																										
- + Get	LANTENNE	0.1u	0.3u	0.5u	291.961n	291.961n																																																																																																										
-That	Performance Function Expression	To	Current	Optimized	Error																																																																																																											
Equates	Valley_X(v(Rch3),1,0)*10^-9	18	20.355	20.355	2.355																																																																																																											
Equates	Valley_Y(v(Rch3),1,1)*10^-3	-40	-42.884	-42.884	-2.884																																																																																																											
Equates	High_X(v(Rch3),1)*10^-9	34	34.293	34.293	293.236m																																																																																																											
Equates	High_Y(v(Rch3),1)*10^-3	100	92.159	92.159	-7.841																																																																																																											
Equates	Low_X(v(Rch3),1)*10^-9	45	46.293	46.293	1.293																																																																																																											
Equates	Low_Y(v(Rch3),1)*10^-3	-95	-88.415	-88.415	6.585																																																																																																											
Equates	Y_Range(v(Rch3),1,1,70n,100n)*10^-3	70	56.224	56.224	-13.776																																																																																																											
Equates	Period(v(Rch3),1,2)*10^-10	290	277.08	277.08	-12.92																																																																																																											
13.7	<table border="1"> <thead> <tr> <th>Find</th> <th>Parameter</th> <th>Low</th> <th>High</th> <th>Step</th> <th>Current</th> <th>Optimized</th> </tr> </thead> <tbody> <tr><td>- + Get</td><td>PUL PULSE(P1)</td><td>7n</td><td>11n</td><td>5n</td><td>10.797n</td><td>10.797n</td></tr> <tr><td>- + Get</td><td>PUL PULSE(P2)</td><td>25n</td><td>29n</td><td></td><td>25n</td><td>25n</td></tr> <tr><td>- + Get</td><td>C1</td><td>20p</td><td>40p</td><td>8p</td><td>24.849p</td><td>24.849p</td></tr> <tr><td>- + Get</td><td>C2</td><td>40p</td><td>90p</td><td>10p</td><td>40p</td><td>40p</td></tr> <tr><td>- + Get</td><td>C3</td><td>6p</td><td>20p</td><td>4p</td><td>16.764p</td><td>16.764p</td></tr> <tr><td>- + Get</td><td>L1</td><td>1.6u</td><td>2.3u</td><td>4u</td><td>2.3u</td><td>2.3u</td></tr> <tr><td>- + Get</td><td>LANTENNE</td><td>0.1u</td><td>0.3u</td><td>0.5u</td><td>275.049n</td><td>275.049n</td></tr> </tbody> </table> <table border="1"> <thead> <tr> <th>-That</th> <th>Performance Function Expression</th> <th>To</th> <th>Current</th> <th>Optimized</th> <th>Error</th> </tr> </thead> <tbody> <tr><td>Equates</td><td>Valley_X(v(Rch3),1,1)*10^-9</td><td>18</td><td>20.98</td><td>20.98</td><td>2.98</td></tr> <tr><td>Equates</td><td>Valley_Y(v(Rch3),1,1)*10^-3</td><td>-40</td><td>-41.95</td><td>-41.95</td><td>-1.95</td></tr> <tr><td>Equates</td><td>High_X(v(Rch3),1)*10^-9</td><td>34</td><td>35.486</td><td>35.486</td><td>1.486</td></tr> <tr><td>Equates</td><td>High_Y(v(Rch3),1)*10^-3</td><td>100</td><td>92.064</td><td>92.064</td><td>-7.936</td></tr> <tr><td>Equates</td><td>Low_X(v(Rch3),1)*10^-9</td><td>45</td><td>49.486</td><td>49.486</td><td>4.486</td></tr> <tr><td>Equates</td><td>Low_Y(v(Rch3),1)*10^-3</td><td>-95</td><td>-90.487</td><td>-90.487</td><td>4.513</td></tr> <tr><td>Equates</td><td>Y_Range(v(Rch3),1,1,70n,100n)*10^-3</td><td>70</td><td>81.694</td><td>81.694</td><td>11.694</td></tr> <tr><td>Equates</td><td>Period(v(Rch3),1,2)*10^-10</td><td>290</td><td>280.795</td><td>280.795</td><td>-9.205</td></tr> </tbody> </table>	Find	Parameter	Low	High	Step	Current	Optimized	- + Get	PUL PULSE(P1)	7n	11n	5n	10.797n	10.797n	- + Get	PUL PULSE(P2)	25n	29n		25n	25n	- + Get	C1	20p	40p	8p	24.849p	24.849p	- + Get	C2	40p	90p	10p	40p	40p	- + Get	C3	6p	20p	4p	16.764p	16.764p	- + Get	L1	1.6u	2.3u	4u	2.3u	2.3u	- + Get	LANTENNE	0.1u	0.3u	0.5u	275.049n	275.049n	-That	Performance Function Expression	To	Current	Optimized	Error	Equates	Valley_X(v(Rch3),1,1)*10^-9	18	20.98	20.98	2.98	Equates	Valley_Y(v(Rch3),1,1)*10^-3	-40	-41.95	-41.95	-1.95	Equates	High_X(v(Rch3),1)*10^-9	34	35.486	35.486	1.486	Equates	High_Y(v(Rch3),1)*10^-3	100	92.064	92.064	-7.936	Equates	Low_X(v(Rch3),1)*10^-9	45	49.486	49.486	4.486	Equates	Low_Y(v(Rch3),1)*10^-3	-95	-90.487	-90.487	4.513	Equates	Y_Range(v(Rch3),1,1,70n,100n)*10^-3	70	81.694	81.694	11.694	Equates	Period(v(Rch3),1,2)*10^-10	290	280.795	280.795	-9.205	
Find	Parameter	Low	High	Step	Current	Optimized																																																																																																										
- + Get	PUL PULSE(P1)	7n	11n	5n	10.797n	10.797n																																																																																																										
- + Get	PUL PULSE(P2)	25n	29n		25n	25n																																																																																																										
- + Get	C1	20p	40p	8p	24.849p	24.849p																																																																																																										
- + Get	C2	40p	90p	10p	40p	40p																																																																																																										
- + Get	C3	6p	20p	4p	16.764p	16.764p																																																																																																										
- + Get	L1	1.6u	2.3u	4u	2.3u	2.3u																																																																																																										
- + Get	LANTENNE	0.1u	0.3u	0.5u	275.049n	275.049n																																																																																																										
-That	Performance Function Expression	To	Current	Optimized	Error																																																																																																											
Equates	Valley_X(v(Rch3),1,1)*10^-9	18	20.98	20.98	2.98																																																																																																											
Equates	Valley_Y(v(Rch3),1,1)*10^-3	-40	-41.95	-41.95	-1.95																																																																																																											
Equates	High_X(v(Rch3),1)*10^-9	34	35.486	35.486	1.486																																																																																																											
Equates	High_Y(v(Rch3),1)*10^-3	100	92.064	92.064	-7.936																																																																																																											
Equates	Low_X(v(Rch3),1)*10^-9	45	49.486	49.486	4.486																																																																																																											
Equates	Low_Y(v(Rch3),1)*10^-3	-95	-90.487	-90.487	4.513																																																																																																											
Equates	Y_Range(v(Rch3),1,1,70n,100n)*10^-3	70	81.694	81.694	11.694																																																																																																											
Equates	Period(v(Rch3),1,2)*10^-10	290	280.795	280.795	-9.205																																																																																																											

VIII. Appendix: Datasheet of the XDRCU-ALT 500/290 kV XLPE Cable



500/290 kV XLPE Cable

Single-core XLPE High Voltage Cable with Aluminium laminated sheath

Cable layout

- *Copper* conductor, stranded, cross-sections of 1000 sqmm and above segmented, optionally with longitudinal water barrier
- Inner semiconductive layer, firmly bonded to the XLPE insulation
- XLPE main insulation, cross-linked
- Outer semiconductive layer, firmly bonded to the XLPE insulation
- *Copper* wire screen with semi-conductive swelling tapes as longitudinal water barrier
- *Aluminium* laminated sheath
- HDPE oversheath, halogen-free, as mechanical protection, optionally: with semi-conductive and/or flame-retardant layer

Production process

The inner semiconductive layer, the XLPE main insulation and the outer semiconductive layer are extruded in a single operation.

Special features of metallic sheath

- *Copper* wire screen as short-circuit current carrying component
- *Aluminium* foil, overlapped, 0,25 mm thick, as radial diffusion barrier
- Low weight, low cost, internationally proven design

Applicable standards

IEC 62067 (2001)

XDRCU-ALT 500/290 kV



Technical data

Copper conductor cross-section		Outer diameter approx. mm	Cable weight approx. kg/m	Capacitance µF/km	Impedance (90°C, 50 Hz) Ω/km	Surge impedance Ω	Min. bending radius mm	Max. pulling force kN
mm ²	kcmil							
630	1250	122	18	0.12	0.22	54	2450	38
800	1600	123	20	0.14	0.20	49	2500	48
1000	2000	127	23	0.16	0.19	47	2550	60
1200	2400	128	24	0.17	0.19	44	2600	72
1400	2750	129	26	0.19	0.18	42	2600	84
1600	3200	135	29	0.19	0.18	42	2700	96
2000	4000	143	34	0.19	0.17	40	2900	120
2500	5000	144	40	0.23	0.17	37	2900	150

Ampacity

Load Factor		Buried in soil 0.7	Buried in soil 1.0	Buried in soil 0.7	Buried in soil 1.0	In free air -	In free air -
mm ²	kcmil	A	A	A	A	A	A
630	1250	954	806	1026	882	1053	1152
800	1600	1076	901	1170	998	1211	1341
1000	2000	1268	1055	1377	1166	1452	1608
1200	2400	1369	1134	1497	1261	1588	1772
1400	2750	1473	1215	1622	1361	1728	1944
1600	3200	1561	1286	1718	1440	1835	2068
2000	4000	1711	1403	1901	1585	2045	2326
2500	5000	1873	1522	2120	1751	2301	2670

Calculation basis:

Conductor temperature 90°C, 50 Hz, soil temperature 25°C, laying depth 1200 mm, soil thermal resistivity 1.0 Km/W, phase distance at flat formation 30 cm, air temperature 35° - Earthing method: Single-end bonding or Cross-bonding